이학박사학위논문

# Mitophagy의 새로운 분자 조절기작에 관한 연구

# A Study on Molecular Mechanism of Novel Mitophagy Regulators

2015년 2월

서울대학교 대학원

생명과학부

박 성 우

# Mitophagy의 새로운 분자조절 기작에 관한 연구

# A Study on Molecular Mechanism of Novel Mitophagy Regulators

지도교수 정 용 근

이 논문을 이학박사 학위논문으로 제출함
2014년 12월

서울대학교 대학원
생명과학부
박 성 우

박성우의 이학박사 학위논문을 인준함
2014년 12월

위 원 장 박 동 은 (인)

부위원장 정 용 근 (인)

위 원 허 원 기 (인)

위 원 손 형 진 (인)

위 원 진 병 관 (인)

# A Study on Molecular Mechanism of Novel Mitophagy Regulators

A dissertation submitted in partial
fulfillment of the requirement for the degree of

**DOCTOR OF PHILOSOPHY**

To the Faculty of
School of Biological Sciences
at
**SEOUL NATIONAL UNIVERSITY**
By
**Sungwoo Park**

Date Approved: December, 2014

_____

_____

_____

_____

_____

# PART Ⅰ

## Choline dehydrogenase interacts with SQSTM1/p62 to recruit LC3 and stimulate mitophagy

# ABSTRACT


## Choline dehydrogenase interacts with SQSTM1/p62 to recruit LC3 and stimulate mitophagy

CHDH (choline dehydrogenase) is an enzyme catalyzing the dehydrogenation of choline to betaine aldehyde in mitochondria. Apart from this well-known activity, I report here a pivotal role of CHDH in mitophagy. Knockdown of CHDH expression impairs CCCP-induced mitophagy and PARK2/parkin-mediated clearance of mitochondria in mammalian cells, including HeLa cells and SN4741 dopaminergic neuronal cells. Conversely, overexpression of CHDH accelerates PARK2-mediated mitophagy. CHDH is found on both the outer and inner membranes of mitochondria in resting cells. Interestingly, upon induction of mitophagy, CHDH accumulates on the outer membrane in a mitochondrial potential-dependent manner. I found that CHDH is not a substrate of PARK2 but interacts with SQSTM1 independently of PARK2 to recruit SQSTM1 into depolarized mitochondria. The FB1 domain of CHDH is

exposed to the cytosol and is required for the interaction with SQSTM1, and overexpression of the FB1 domain only in cytosol reduces CCCP-induced mitochondrial degradation via competitive interaction with SQSTM1. In addition, CHDH, but not the CHDH FB1 deletion mutant, forms a ternary protein complex with SQSTM1 and MAP1LC3 (LC3), leading to loading of LC3 onto the damaged mitochondria via SQSTM1. Further, CHDH is crucial to the mitophagy induced by MPP+ in SN4741 cells. Overall, my results suggest that CHDH is required for PARK2-mediated mitophagy for the recruitment of SQSTM1 and LC3 onto the mitochondria for cargo recognition.

*Key word*: Choline dehydrogenase, LC3, mitophagy, SQSTM1/p62, PARK2/parkin

Student Number : 2009-30857

# TABLE OF CONTENTS

# LIST OF FIGURES

# 1. INTRODUCTION

CHDH is an enzyme catalyzing the dehydrogenation of choline to betaine aldehyde in the mitochondria.[1] Betaine aldehyde is subsequently converted to betaine, an important methyl donor for the synthesis of methionine from homocysteine.[2, 3] CHDH has been highlighted by Ma *et al.,* who report that CHDH is overexpressed in patients with a favorable outcome associated with tamoxifen monotherapy in a cohort of early-stage estrogen receptor-positive breast cancer patients.[4] In addition, a population-based study shows that CHDH expression correlates with ESR (estrogen receptor) and HER2 status and is regulated by estrogen in an ESR-dependent manner.[5] A recent study demonstrates that CHDH plays a pivotal role in mitochondrial function in several tissues, with the most striking effects in sperm of *chdh*$^{-/-}$ mice.[6] Several single nucleotide polymorphisms (SNPs) of CHDH are common in humans. Between 42 to 47% of the population carrying one allele of the rs12676 SNP shows liver and muscle dysfunction when fed a choline-deficient diet.[7, 8] Moreover, this SNP affects

the motility and mitochondrial morphology of human sperm.[9]

Mitochondrial quality control is performed within certain steps along with the level of damage.[10] Cells must eliminate mitochondria when they fail to repair their components using proteolytic systems or ROS regulation. Autophagic machineries are employed in this type of organellar-level mitochondrial degradation, termed 'mitophagy,' which is critical for the maintenance of cellular homeostasis and survival.[11] Autophagy is responsible for the initial flux of mitophagy, and the two processes share the same pathway, including ULK1, ATG13,[12, 13] MAP1LC3B/LC3B (refer to LC3 hereafter), and BECN1/Beclin1[14] with a controversy in case of BECN1.[15] Inhibition of MTORC1 is also required for autophagy and mitophagy.[16] However, it remains unclear which critical factor targets autophagic machineries to the mitochondria. In recent years, PINK1/PARK6 (PTEN induced putative kinase 1) and PARK2/parkin (parkin RBR E3 ubiquitin protein ligase) have emerged as a pivotal paradigm of mitophagic process. These genes are mutated in autosomal recessive Parkinson disease (PD)[17, 18] and contribute to regulation of mitochondrial integrity,

including mitophagy.[14] PINK1 has a short half-life and is rapidly degraded under steady-state conditions by proteases located in the inner membrane (IM) of mitochondria. However, once the mitochondrial membrane potential has dissipated, it becomes stable and recruits PARK2.[19, 20] The ubiquitin-ligase activity of PARK2 is then activated[21] and promotes ubiquitination of mitochondrial proteins, driving mitophagy. Although the mechanism of mitophagy has been intensively studied,[22-24] the mitophagy-specific factors remain unclear.

In this study, I assess the role of CHDH in PARK2-mediated mitophagy. Beyond its well-known role in betaine production, I demonstrate that CHDH is required for mitophagy in which CHDH interacts with SQSTM1, a mitophagic adaptor molecule, and subsequently facilitates the recruitment of LC3 into the mitochondria.

# 2. MATERIALS AND METHODS

## 2.1. Cell culture and transfection

HeLa, HEK293T and SH-SY5Y cells were grown in DMEM (Hyclone, SH30243.01) supplemented with 10% fetal bovine serum (Hyclone, SH30919.03), 50 U/mL penicillin and 50 μg/mL streptomycin at 37 ℃ under 5% $CO_2$. SN4741 dopaminergic neuronal cells were cultured as described previously.[28] Stable cell lines were generated after selection with G418 (1 mg/mL; Invitrogen, 10131027) for 2 weeks following DNA transfection and confirmed by western blot analysis. *sqstm1* MEFs were gifted by Dr. J. Shin (Sungkyunkwan University, Korea). DNA, shRNA and siRNA transfections were performed with Polyfect reagent (Qiagen, 1015586) and Lipofectamine 2000 reagent (Invitrogen, 11668019) for 24 and 48 h, respectively, according to the manufacturer's instructions.

## 2.2. Plasmids and siRNA

*CHDH* shRNA constructs were generated in pSUPER-neo (OligoEngine, VEC-PBS-0004) using the following target sequence for human *CHDH*: 5′-CCA CAT TCA GTC AGA TAA A-3′ and for mouse *Chdh*: 5′-GGT AAT GAT TGC AGA GAA A-3′. Serial deletion (Δ) mutants of *CHDH* were generated by excising the FB1 domain (115 to 978) (CHDH-FB1Δ), RD domain (997 to 1545) (CHDH-RDΔ) and FB2 domain (1531 to 1722) (CHDH-FB2Δ) based on the bioinformatic domain prediction using MITOPROT (http://ihg.gsf.de/ihg/mitoprot.html) and SUPERFAMILY Sequence Search (http://supfam.org/SUPERFAMILY/hmm.html). The HA-CHDH and CHDH-MYC-HIS were produced by subcloning CHDH into pcDNA3-HA and pEF1/MYC-HIS (Invitrogen, V92120), respectively. HA-CHDH-MYC-HIS was constructed by subcloning CHDH-MYC-HIS into pcDNA3-HA for HA tagging at the N terminus and MYC-HIS tagging at the C terminus. The SQSTM1-FL-MYC-HIS, SQSTM1-PB1Δ-MYC-HIS were gifts from Dr. M. Tanaka (Kyoto Prefectural University, Japan) and PINK1-GFP was from Dr. J. Chung (Seoul National University, Korea). TOMM20-GFP, TOMM20-FB1-GFP and FB1-GFP were constructed by

subcloning of *TOMM20* and/or the FB1 domain cDNA into pEGFP-N1 (Invitrogen, 6085-1). Rs12676 SNP mutant of CHDH (R78L) was generated by site-directed mutagenesis using PCR: The following primers were used. Fwd, 5′-GCC CAA GGA CGT GCT CGC GGG GAG CAA GCG-3′ and Rev, 5′-CGC TTG CTC CCC GCG AGC ACG TCC TTG GGC-3′. The *SQSTM1* siRNA was kindly provided by Dr. J. Shin (Sungkyunkwan University, Korea).

## 2.3. Measurement of Mito-GFP intensities

After transfection with Mito-GFP, the fluorescence of cells was measured with EnVision multilabel plate reader (PerkinElmer, 940 Winter Street, Waltham, 02451, MA USA).

## 2.4. Measurement of enzyme activity and LC-MS

Mitochondria were purified from cells using differential centrifugation as described previously.[20] After resuspension in reaction buffer (10 mM sodium

phosphate, 10 mM Tris-Cl, pH 8.0), mitochondria were burst by sonication and then mixed with 10 mM choline chloride and 2 mM phenazine methosulfate. The reaction was incubated at 37 °C for 1 h in the dark and samples were subjected to ultracentrifugation at 100,000 g for 30 min to precipitate mitochondrial debris; the supernatant fraction was kept at -70 °C until analysis. For LC-MS analysis, a Thermo-Finnigan Surveyor instrument (Thermo Scientific, USA), equipped with autosampler and PDA-UV detector and Thermo-Finnigan LCQ Deca XP plus ion trap mass spectrometer with electrospray ionization interface was used. ZoRBAX 300SB-C8 P/No. 865750-906, size 2.1 x 50 mm, 3.5 µm, S/No. USACR01562 was used for chromatographic separations. The injection volume was 10 µL and the mobile phase consisted of 0.1% formic acid in distilled water (A) and in acetonitrile (B). Gradient elution at a flow rate of 150 µL/min was as following: 95% (A) and 5% (B) from 0 to 20 min, 5% (A) and 95% (B) from 20 min to 25 min, and returned to the initial condition from 20 min to 30 min. Total running time was 30 min. Ionization of analytes was carried out using electrospray ionization. The capillary temperature was

maintained at 275 °C. The ion source voltage and the nebulizer gas were set at 5 kV and 30 units, respectively. The capillary voltage was at 46 V in positive and -15 V in negative ionization mode. The average scan time was 0.01 min while the average time for changing polarity was 0.02 min. The collision energy was generally chosen in order to maintain about 35% abundance of the precursor ion.

## 2.5. Immunoprecipitation, western blot and antibodies

Immunoprecipitation and western blot analysis were performed as reported previously.[51] Briefly, cells were lysed in lysis buffer (20 mM Tris-Cl, pH 7.6, 150 mM NaCl, 1% Triton X-100) and clarified by centrifugation. Cell lysates were dichotomized for immunoprecipitation and whole cell lysate quantification. For immunoprecipitaion, primary antibody was added overnight at 4 °C and pulled down by protein G Sepharose beads (GE Healthcare, 17-0618-01) at 4 °C for 1 h. Both samples were boiled in 1 X SDS sample buffer, separated by SDS-PAGE and transferred onto nitrocellulose membrane (Pall Corporation, 66485). After blocking

with 5% skim milk in TBST, the membrane was incubated with the following antibodies: CHDH (Santa Cruz, sc-102442), TOMM20 (sc-17764), GFP (sc-8334), MYC (sc-40), TUBA/tubulin, alpha (sc-23948) and ACTB (sc-47778) SOD2 (Upstate, 06-984), COX4I1 (Abcam, ab14744-100), SQSTM1 (Abnova, H00008878-M01 and Santa Cruz, sc-25575), PARK2 (Abcam, ab77924 and Santa Cruz, sc-32282), LC3 (Novus, NB100-2220), FLAG (Sigma, F3165) and TIMM23 (BD Bioscience, 611222).

## 2.6. Immunofluorescence and colocalization coefficient

Cells were fixed with 4% paraformaldehyde and permeabilized with 0.005% digitonin in PBS (Gibco, 70011-044). After blocking with 10% fetal bovine serum, the fixed cells were incubated with antibodies at 1:100 to 1:250 dilution ratio, followed by incubation with Alexa Fluor secondary antibodies (Molecular Probes, A11005, A11001, A11008 and A11012). Samples were visualized under a confocal laser scanning microscope (Carl Zeiss, LSM700, Carl-Zeiss-Promenade 10, 07745, Jena

Germany) and colocalization coefficient was analyzed using ZEN software (Carl Zeiss).

## 2.7. Flow cytometry

Cells were harvested and monocellized with Trypsin-EDTA, followed by fixation with 70% ethanol with voltexing and then subjected to analysis using a FACSCalibur flow cytometer (BD biosciences, 1 Becton Drive Franklin Lakes, 07417, NJ USA) according to the manufacturer's instructions.

## 2.8. Mitochondrial DNA quantification

Mitochondrial DNA was extracted using Exprep kit (GeneAll, 101-102) and subjected to PCR analysis using *MT-CYB* primers: Fwd, 5′-TTC TGA GGG GCC ACA GTA ATT ACA AAC TTA-3′, Rev, 5′-ATG GAG GAT GGG GAT TAT TGC TAG GAT GAG-3′. Prior to mitochondrial DNA extraction, whole cell DNA was also extracted for quantification as described previously[52] and subjected to PCR analysis

using *ACTB* primers: Fwd, 5′-CGT TGG CAT CCA CGA AAC TA-3′, Rev, 5′-AGT ACT TGC GCT CAG GAG GA-3′.

## 2.9. Mitochondria fractionation

Cells were resuspended in PBS and subjected to sonication twice at 30% amplitude for 3 sec with an Ultrasonic Processor 130 W (Sonics & Materials, 53 Church Hill Road, Newtown, 06470-1614, CT USA). Unbroken cells and nuclei were removed by centrifugation at 1,000 g for 10 min. The postnuclear supernatant fraction was pelleted by further centrifugation at 10,000 g for 15 min to obtain the mitochondria pellet. For submitochondria fractionation, the pelleted mitochondria were rinsed with swelling buffer (10 mM $KH_2PO_4$, pH 7.4) once and resuspended in swelling buffer for 20 min with gentle mixing, followed by addition of an equal volume of shrinking buffer (10 mM HEPES, pH 7.4, 32% sucrose, 30% glycerol, 10 mM $MgCl_2$) for 15 min. Subsequent centrifugation at 10,000 g for 15 min yielded the pelleted mitoplast and suspended OM and intermembrane space (IMS) fraction which

was kept for further separation. The mitoplast was rinsed twice with washing buffer (250 mM sucrose, 1 mM EGTA, 10 mM HEPES, pH 7.4), resuspended in swelling buffer and burst 5 times by sonication at 50% amplitude for 3 sec. this suspension was centrifuged at 12,000 g for 15 min to discard the unbroken mitoplast. Finally, samples were processed by ultracentrifugation at 100,000 g for 40 min to separate OM and IMS fractions, and the IM matrix fractions. Every procedure was performed at 4 °C.

### 2.10. Proteinase K degradation assay

For proteinase K degradation assay, the purified mitochondria were resuspended in PK assay buffer (20 mM HEPES, pH 7.4, 250 mM sucrose, 80 mM potassium acetate, 5 mM magnesium acetate) and added with proteinase K (GenDepot, P2170-005) or control BSA in ice. After 10 min, the digestion was stopped with addition of 1 mM PMSF.

# 3. RESULTS

### 3.1. CHDH is required for PARK2-mediated mitophagy

First, I examined the necessity of CHDH for mitophagy induced by carbonyl cyanide *m*-chlorophenylhydrazone (CCCP), a mitochondrial uncoupler that triggers mitochondrial depolarization and mitophagy.[25] By using *CHDH* shRNA, I generated stable HeLa cells that showed reduced expression of *CHDH* (HeLa-sh*CHDH* cells) (**Fig. 1B**, upper). As has been previously reported[26], immunofluorescence analysis revealed that CCCP treatment induced the degradation of TOMM20-positive mitochondria in the presence of PARK2 in control HeLa cells (**Fig. 1A**, left), which contain no endogenous PARK2. However, knockdown of CHDH expression impeded the degradation of mitochondria (**Fig. 1A**, right). Mitochondrial degradation did not occur in the absence of PARK2, consistent with the previous report.[11, 27] When flow cytometry analysis was employed to measure the total fluorescence intensity of Mito-RFP, the results of CCCP exposure showed that clearance of Mito-RFP-positive

mitochondria was also retarded in HeLa-sh*CHDH* cells (**Fig. 2A**). Similarly, quantification of the degradation of mitochondrial DNA and proteins revealed that quantities of *MT-CYB/cytochrome b* DNA and mitochondrial proteins, such as SOD2/MnSOD and TOMM20, were less reduced in HeLa-sh*CHDH* cells than in control cells during mitophagy (**Fig. 2B, C**). These results indicate that CHDH is required for the proper functioning of PARK2-mediated mitophagy in HeLa cells.

Given that PARK2-mediated mitophagy is related to PD, I also examined the role of CHDH in mitophagy of SN4741 neuronal cells, a clonal substantia nigra dopaminergic neuronal murine cell line which expresses PARK2.[28] Using western blot analysis, I confirmed the expression of PARK2 in SN4741 cells (data not shown). Exposure of SN4741 cells to CCCP resulted in clearance of Mito-RFP-positive mitochondria (**Fig. 2D, E**). On the contrary, knockdown of CHDH expression significantly impaired the clearance of Mito-RFP-positive mitochondria in SN4741 cells (**Fig. 2D, E**), suggesting that CHDH is required for PARK2-mediated mitophagy not only in HeLa cells but also in SN4741 dopaminergic neuronal cells.

I also examined the effect of CHDH overexpression on mitophagy. When HeLa cells expressing PARK2 were exposed to CCCP, colocalization of GFP-LC3 and Mito-RFP was enhanced by CHDH overexpression (**Fig. 3A**). Interestingly, CHDH overexpression followed by CCCP treatment also increased the colocalization of mitochondria and LC3. When I analyzed mitochondrial DNA and protein quantities following CCCP treatment, I found that clearance of *MT-CYB* DNA and mitochondrial COX4I1/COX-IV protein was accelerated by CHDH overexpression (**Fig. 3B**, **C**). Consistent with this result, the fluorescence intensity of Mito-GFP was rapidly dissipated by CHDH overexpression in HEK293T cells during mitophagy, which is almost equivalent to that by PINK1 overexpression (**Fig. 3D**). These results indicate that CHDH overexpression enhances CCCP-induced clearance of mitochondria. However, expression level of CHDH did not affect the stability of PINK1 protein, although CCCP treatment stabilized PINK1 in mitochondria as previously reported (**Fig. 4A**, **B**).[29, 30] In addition, PINK1 knockdown attenuated CCCP-induced mitophagy in both control cells and cells overexpressing CHDH. However, the

overexpression of CHDH still enhanced mitophagy in PINK1 knockdown cells (**Fig. 4C**).

### 3.2. Mitophagic activity of CHDH is independent of enzyme activity

I next examined whether this mitophagic activity of CHDH is related to its enzymatic activity that converts choline to betaine aldehyde. I constructed a series of CHDH deletion mutants based on bioinformatic analysis (materials and methods). CHDH appears to have a mitochondria-targeting sequence at its N-terminus (residues 1 to 38) and three functional domains, named FAD/NAD(P)-binding domain 1 (FB1, residues 39 to 326), FAD-linked reductase domain (RD, residues 333 to 515) and FAD/NAD(P)-binding domain 2 (FB2, residues 511 to 574) (**Fig. 5**). Expression of these constructs was confirmed by western blot analysis (**Fig. 6A**). Overexpression of the CHDH-RDΔ or CHDH-FB2Δ mutants induced colocalization of GFP-LC3 with Mito-RFP as effectively as wild-type CHDH, but the CHDH-FB1Δ mutant failed to do so (**Fig. 6B**, **Fig. 7A**), indicating that the FB1 domain of CHDH is critical for its

mitophagy-stimulating activity. However, enzyme activity assays using these mutants illustrated that all of these CHDH mutants exhibited impaired activity of the enzyme that generates betaine aldehyde; the FB1 and FB2 domains were crucial for this activity, as was the RD domain, which was less important but still required (**Fig. 7B**). Further, when I tested the mitophagic activity of betaine, the product of CHDH and betaine aldehyde dehydrogenase, which is involved in many biochemical pathways,[31] I discovered that betaine did not affect the colocalization of LC3 with mitochondria (**Fig. 8**). Overall, it appears that the mitophagy-stimulating function of CHDH is independent of its well-known enzymatic activity and enzymatic product.

### 3.3. CHDH accumulates on the outer membrane following mitochondrial damage

I next investigated the subcellular location of CHDH. Consistent with the previous reports,[32, 33] I found that CHDH was present in mitochondria (**Fig. 9A**). I further assessed the submitochondrial location of CHDH using a submitochondrial

fractionation assay (**Fig. 9B**). CHDH and the outer membrane (OM)-located TOMM20 were detected in the OM fraction, as well as in the IM fraction, in which COX4I1 was also located (**Fig. 9B**). However, CHDH was not detected in the cytosol and matrix fractions. To confirm this result, I purified mitochondria from HeLa and HEK293T cells and performed a proteinase K (PK) degradation assay. Incubation of the purified mitochondria with the increased concentrations of PK resulted in gradual degradation of CHDH and TOMM20, but it did not affect the levels of SOD2 in the matrix or IM-localized COX4I1 (**Fig. 9C**). Whereas the previous study proposed that CHDH is located on the IM of mitochondria, these results indicate that CHDH is present on both the OM and IM of mitochondria. According to the western blot analysis showing that CHDH was retained in the membrane-associated fractions after the treatment with high salt (**Fig. 10A**), I believe that CHDH is present as a transmembrane protein in the mitochondria.

Next, I compared the quantity of CHDH on the OM and IM of mitochondria following CCCP treatment. Instead of using the conventional concentration (10 to 20

μM) of CCCP, which induces mitochondrial membrane potential dissipation but may interfere with membrane integrity and thus result in marker protein contamination in PK and fractionation assays, I used a lower concentration of CCCP that would induce mild mitochondrial depolarization but not affect membrane integrity during the assays. To determine the required concentration, I assessed different concentrations of CCCP, ranging from 0.01 to 10 μM of CCCP, in pilot experiments and found that 0.1 μM CCCP was sufficient to induce significant depolarization of the mitochondrial membrane (**Fig. 10B**). Using this concentration of CCCP, I found that in mitochondria isolated from CCCP-treated cells, CHDH was more sensitive to degradation by PK than it was in mitochondria isolated from untreated control cells (**Fig. 11A**). I thus hypothesized that CHDH accumulates on the OM of mitochondria following the loss of the mitochondrial membrane potential. A subsequent fractionation assay also showed that CCCP treatment induced the accumulation of CHDH in the OM fraction, with a concomitant reduction of CHDH in the IM fraction (**Fig. 11B, C**). I also performed an assay using cycloheximide to block protein translation, which showed

that CHDH accumulated on the OM of mitochondria in the presence of cycloheximide (**Fig. 11B**), indicating that the accumulation of CHDH on the OM of mitochondria does not result from *de novo* protein synthesis.

When I assessed the topology of CHDH in the mitochondrial membrane, a PK assay following the expression of N-terminal-tagged CHDH (HA-CHDH) revealed that the N terminus of CHDH may be exposed to the cytosol in control cells (**Fig. 12A**). I confirmed this result with immunocytochemical analysis. In a control analysis, an immunofluorescence assay following differential permeabilization of cells revealed that the immunofluorescent signal of TOMM20, but not SOD2, was detectable by mild permeabilization using 0.001% digitonin. In contrast, immunofluorescence of both TOMM20 and SOD2 were observed after permeabilization with 0.05% Triton X-100, which permeabilizes both the plasma membrane and the mitochondrial membrane (**Fig. 12B**, upper). Identical experiments were then performed following the expression of dual-tagged HA-CHDH-MYC-HIS containing HA at the N terminus and MYC-HIS at the C terminus. In contrast to the N-terminal HA,

immunofluorescence of the C-terminal HIS was not observed after permeabilization with 0.001% digitonin but observed with Triton X-100 (**Fig. 12B**, lower). These results suggest that the N terminus of OM-located CHDH is exposed to the cytosolic side, whereas the C terminus is located inside mitochondria in both control and CCCP-treated cells. Further, western blot analysis using CHDH antibody recognizing the C terminus revealed that approximately 45-kDa cleavage product of CHDH appeared in a PK assay of purified mitochondria and its amount was increased by CCCP treatment in SH-SY5Y cells (**Fig. 12C**). Thus, approximately a 20-kDa N-terminal region of CHDH is exposed to the cytosol.

To further assess the mechanism by which CHDH translocates across the mitochondrial membranes, I hypothesized that the mitochondrial OM–IM contact site was a candidate site for the CHDH path. Because the VDAC1-adenine nucleotide translocator (ANT) complex is one of the contact sites,[34] I tested whether VDAC1 functions as a path for CHDH during mitophagy. Interestingly, I found that CHDH interacted with VDAC1 following CCCP treatment (**Fig. 13A**). Moreover, compared

to controls, overexpression of VDAC1 increased PK-sensitive cleavage of CHDH during mitophagy (**Fig. 13B**), indicating that the accumulation of CHDH on the OM is enhanced by VDAC1. Thus, the VDAC1-ANT complex may function to regulate the accumulation of CHDH in the OM of mitochondria during mitophagy. On the other hand, this accumulation was not affected by the overexpression of PLSCR3 (phospholipid scramblase 3) (**Fig. 13C**), which plays a role in the externalization of cardiolipin to the OM of mitochondria during mitophagy.[35] Also, total amount of CHDH protein was not changed during mitophagy or by PINK1 knockdown (**Fig. 13D**).

### 3.4. CHDH interacts with SQSTM1 independently of PARK2 during mitophagy

Because knockdown of CHDH expression resulted in reduced colocalization of LC3 with mitochondria (**Fig. 8**), I hypothesized that CHDH may affect the cargo recognition step in mitophagy via SQSTM1, an important adaptor that connects damaged cargo to LC3.[36, 37] Using immunoprecipitation analysis,I observed that

CHDH interacted with SQSTM1 in the transfected cells (**Fig. 14A**). Interestingly, this interaction remarkably increased in cells following CCCP treatment. Similarly, endogenous CHDH bound to SQSTM1 in SH-SY5Y neuronal cells and this interaction also increased following exposure to CCCP; the interaction reached a maximum level at 30 min and remained high up to 240 min (**Fig. 14B**). However, CHDH did not interact with other mitochondrial proteins, such as TOMM20 and COX4I1. I confirmed the endogenous interaction using a reciprocal immunoprecipitation assay (**Fig. 14C**).

I then addressed whether this interaction was dependent on PARK2 in HeLa cells. Although PARK2 expression is absent in HeLa cells, a basal level of the interaction between CHDH and SQSTM1 was also detected in HeLa cells, and this interaction increased following CCCP treatment (**Fig. 15A**). However, the interaction was impaired in HeLa-sh*CHDH* cells compared to control HeLa cells. Moreover, the overexpression of PARK2 in HeLa cells did not affect the interaction (**Fig. 15B**), indicating that the binding of CHDH to SQSTM1 is independent of PARK2. Further,

when I examined PARK2-mediated ubiquitination of mitochondrial proteins during mitophagy, I observed the ubiquitination of VDAC1, a substrate of PARK2,[26] but not of CHDH (**Fig. 15C**), indicating that CHDH is not a substrate of PARK2.

Next, I determined the domains responsible for the interaction between CHDH and SQSTM1 using deletion mutants (**Fig. 5** and **16A**). The results of an immunoprecipitation assay showed that, unlike full-length SQSTM1, a SQSTM1-PB1Δ mutant lacking the PB1 domain, which is responsible for its interaction with certain aggregate-prone mutant proteins,[38, 39] failed to interact with CHDH in HEK293T cells (**Fig. 16B, C**). I also determined the binding region of CHDH and observed that the CHDH-FB1Δ mutant lacking an FB1 domain did not interact with SQSTM1 (**Fig. 16D**). These results suggest that the PB1 domain of SQSTM1 and the FB1 domain of CHDH are required for their interaction. I confirmed these results using a colocalization assay under a confocal microscope. Unlike wild-type CHDH, mutant CHDH-FB1Δ did not colocalize with SQSTM1 in cells before or after CCCP treatment (**Fig. 17A**). Expression of CHDH or CHDH-FB1Δ did not affect the

function of PARK2, as examined by VDAC1 ubiquitination (**Fig. 17B**). SNPs of CHDH, especially rs12676 (G233T; R78L), which is located in the FB1 domain, are known to be responsible for mitochondrial function and morphology in mice and humans, especially in sperm.[6,9] When this SNP was examined for its ability to interact with SQSTM1, there was no significant difference between CHDH wild-type and rs12676 (**Fig. 17C**).

### 3.5. The interaction of CHDH with SQSTM1 brings LC3 to damaged mitochondria for cargo recognition during mitophagy

To investigate the functional significance of the interaction between CHDH and SQSTM1 during mitophagy, I examined knockdown effects of CHDH expression on SQSTM1 recruitment into impaired mitochondria. Compared to HeLa control cells, colocalization between Mito-RFP and SQSTM1 was abrogated in HeLa-CHDH knockdown cells during mitophagy (**Fig. 18A**, **B**). In addition, a mitochondrial fractionation assay illustrated that SQSTM1 was dramatically recruited into the

mitochondrial fraction as early as 15 min after CCCP treatment in SH-SY5Y cells and resided in mitochondria for up to 60 min (**Fig. 19A**). Strikingly, this recruitment was much reduced in SH-SY5Y-CHDH knockdown cells. However, CHDH did not affect the recruitment of PARK2 into mitochondria. To further investigate the recruitment of SQSTM1 to damaged mitochondria, I performed a fractionation assay. Compared to untreated control cells, CCCP treatment increased the quantity of mitochondrial fraction-localized SQSTM1 in HEK293T cells overexpressing CHDH, but not in cells expressing the SQSTM1 binding-defective CHDH-FB1Δ mutant (**Fig. 19B**).I also found that the degradation of mitochondrial proteins during mitophagy was partially but significantly impaired by SQSTM1 knockdown in HEK293T cells (**Fig. 19C**). These observations suggest that CHDH is required for the recruitment of SQSTM1 into damaged mitochondria for degradation.

Further, confocal imaging analysis revealed that the colocalization of GFP-LC3 and Mito-RFP was decreased by 2-fold in HeLa-sh*CHDH* cells compared to HeLa control cells (**Fig. 20A**). This reduction in the colocalization was also observed in

HeLa control cells lacking PARK2 (**Fig. 20A**, lanes 2 and 6). It thus appears that CHDH recruits LC3 independently of PARK2, as was observed in the SQSTM1-binding pattern of CHDH. Given that SQSTM1 directly links damaged and ubiquitinated mitochondria to LC3,[36] I examined protein complex formation among CHDH, SQSTM1 and LC3. The results of an immunoprecipitation assay showed that CHDH, but not CHDH-FB1Δ, formed a protein complex with SQSTM1 and LC3 in HeLa cells following CCCP treatment (**Fig. 20B**). Under identical conditions, knockout of SQSTM1 expression prevented formation of the ternary protein complex containing LC3 and CHDH (**Fig. 20C**). Because an LC3-containing autophagosome fused with a lysosome is destined for degradation, I then examined the relative effects of CHDH and CHDH-FB1Δ on PARK2-dependent degradation of mitochondria. Immunofluorescence analysis revealed that CHDH-FB1Δ was less effective than CHDH to clear TOMM20-positive mitochondria following CCCP treatment (40.8% vs. 60.5%) (**Fig. 20D**). These results suggest that CHDH binds to SQSTM1 to bring LC3 to the damaged mitochondria for the degradation of mitochondria and is

indispensable for PARK2-mediated mitophagy at the cargo-recognition step.

Based on the domain mapping results for CHDH, I asked whether the CHDH FB1 domain is sufficient for LC3 recruitment into mitochondria. I generated a TOMM20-FB1-GFP chimera, a mitochondrial OM-targeting chimeric construct containing TOMM20 fused to CHDH FB1-GFP (**Fig. 21A**, upper), and examined its ability to recruit LC3 into the mitochondria under a confocal microscope. When these constructs were overexpressed in HeLa cells, no difference was observed between TOMM20-GFP and TOMM20-FB1-GFP in the recruitment of mRFP-LC3 into mitochondria. However, when cells were exposed to CCCP, TOMM20-FB1-GFP increased colocalization of mRFP-LC3 with the mitochondria by 2-fold, compared to TOMM20-GFP (**Fig. 21A**, lower). These observations suggest that the CHDH FB1 domain is necessary for LC3 recruitment to damaged mitochondria.

In addition, I addressed whether the interaction between CHDH and SQSTM1 is critical for mitophagy using a competition assay. I found that FB1-GFP could bind to SQSTM1 in the transfected cells during mitophagy, although the interaction appears to

be weak (**Fig. 21B**). Moreover, ectopic expression of FB1-GFP weakened the interaction between CHDH and SQSTM1 in a dose-dependent manner. I then assessed the effect of FB1-GFP on mitochondrial clearance during mitophagy. Immunofluorescence analysis revealed that ectopic expression of FB1-GFP significantly inhibited PARK2-dependent clearance of TOMM20-positive mitochondria during CCCP-induced mitophagy (from 51.8% to 19.0%) (**Fig. 22A, B**). Consistently, FB1-GFP colocalized with SQSTM1-MYC in the transfected cells (**Fig. 22C**). These results suggest that the interaction between CHDH and SQSTM1 is important for mitophagy to proceed.

### 3.6. CHDH is implicated in MPP+-induced mitophagy in SN4741 dopaminergic cells

The failure of appropriate recognition of damaged mitochondria causes accumulation of defective mitochondria[11, 26] and this failure is closely associated with the pathogenesis of PD.[40] In SN4741 dopaminergic cells, I thus addressed the role of

CHDH during mitophagy triggered by 1-methyl-4-phenylpyridinium (MPP+), a Parkinsonism-causing reagent.[41] Like CCCP, treatment with MPP+ induced a significant level (30.0%) of colocalization of GFP-LC3 with mitochondria in SN4741 cells (**Fig. 22D**). In contrast, downregulation of CHDH expression abolished the colocalization (8.5%). These results indicate that CHDH is essential in the mitophagy of SN4741 dopaminergic neurons following exposure to MPP+.

**Figure 1. CHDH is required for CCCP-induced mitophagy.**

(**A, B**) HeLa-Control (Ctrl) and HeLa-CHDH knockdown (HeLa-sh*CHDH*) stable cells were transfected with FLAG-Ctrl or FLAG-PARK2 and then exposed to DMSO or 10 μM CCCP for 24 h. After staining with TOMM20 antibody and Hoechst 33258 dye, cells were examined under a confocal microscope. Scale bar = 10 μM (**A**). Expression of CHDH in HeLa-Ctrl and HeLa-sh*CHDH* cells was assessed using western blot analysis (**B**, upper). The signal intensity of TOMM20 in HeLa-Ctrl and HeLa-sh*CHDH* cells ($n > 50$) exposed to CCCP and expressing PARK2 in (**A**) were quantified using the ImageJ program and are represented as bars with the mean ± S.D, * $P < 0.05$ (**B**, lower).

**Figure 1**

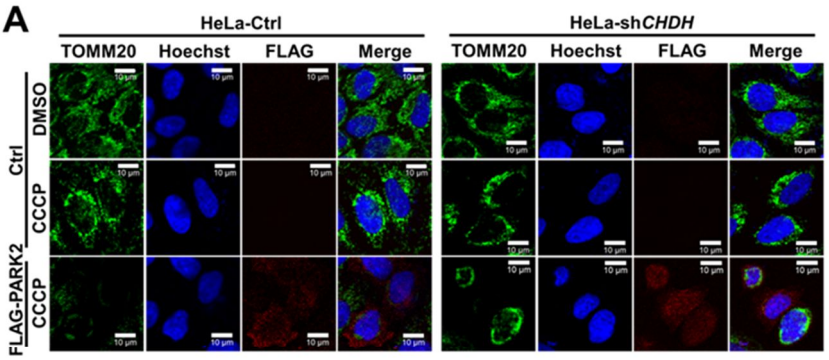
A
HeLa-Ctrl
HeLa-shCHDH
TOMM20
Hoechst
FLAG
Merge
Ctrl
DMSO
CCCP
FLAG-PARK2
CCCP
10 μm

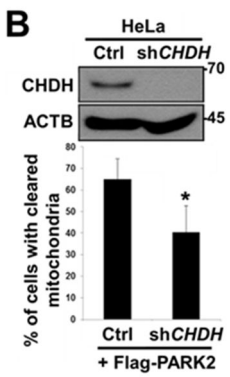
B
HeLa
Ctrl
shCHDH
CHDH
ACTB
70
45
% of cells with cleared mitochondria
80
70
60
50
40
30
20
10
0
*
Ctrl
shCHDH
+ Flag-PARK2

**Figure 2. CHDH is required for CCCP-induced and PARK2-mediated mitophagy.**

(**A**) HeLa-Ctrl and HeLa-sh*CHDH* cells were transfected with PARK2 and Mito-RFP and treated with DMSO or 10 μM CCCP. After 24 h, cells were fixed and subjected to flow cytometry analysis, as described in the materials and methods.

(**B, C**) HeLa-Ctrl and HeLa-sh*CHDH* cells were transfected with PARK2 and then left untreated or exposed to 10 μM CCCP for 24 h. Mitochondrial DNA and proteins were extracted and subjected to PCR analysis using synthetic primers for *cytochrome b* (*MT-CYB*) and *ACTB* (D), and western blot analysis using SOD2 and TOMM20 antibodies (**C**), respectively.

(**D, E**) SN4741 cells were transiently transfected with Mito-RFP and either pSuper (Ctrl) or *CHDH* shRNA and then exposed to DMSO or 20 μM CCCP. After 24 h, cells were stained with Hoechst 33258 dye and examined under a confocal microscope. Scale bar = 10 μM (**D**). The signal intensities of Mito-RFP in CCCP-treated control and CHDH knockdown cells were quantified as in (**Fig. 1B**) and are represented as %

of cells ($n$ > 50) with cleared mitochondria. Bars represent the mean ± S.D. * $P$ < 0.001 (**E**). TUBA, tubulin, alpha.

Figure 2

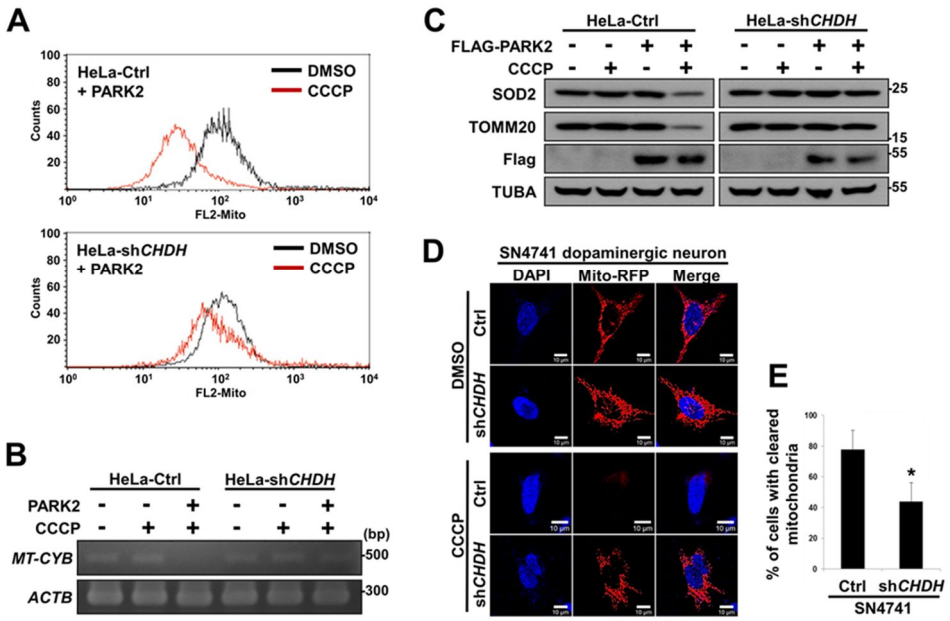
A
HeLa-Ctrl
+ PARK2
DMSO
CCCP
Counts
FL2-Mito
HeLa-shCHDH
+ PARK2
B
HeLa-Ctrl
HeLa-shCHDH
PARK2
CCCP
(bp)
MT-CYB
ACTB
500
300
C
HeLa-Ctrl
HeLa-shCHDH
FLAG-PARK2
CCCP
SOD2
TOMM20
Flag
TUBA
25
15
55
55
D
SN4741 dopaminergic neuron
DAPI
Mito-RFP
Merge
DMSO
CCCP
Ctrl
shCHDH
E
% of cells with cleared mitochondria
Ctrl
shCHDH
SN4741

**Figure 3. Overexpression of CHDH accelerates mitochondrial clearance.**

(**A**) HeLa-Ctrl and HeLa-CHDH cells were cotransfected with GFP-LC3, Mito-RFP and either GFP control vector (Ctrl) or PARK2 and then incubated with 10 μM CCCP. After 2 h, cells were analyzed under a confocal microscope; the colocalization coefficient (%) of GFP-LC3 and Mito-RFP is shown with bars representing the mean ± S.D ($n > 50$). * $P < 0.001$.

(**B, C**) HeLa-Ctrl and HeLa-CHDH cells were left untreated or exposed to 10 μM CCCP for 30 h (B) or for the indicated times (**C**). Mitochondrial DNA (*MT-CYB*) and proteins (CHDH, COX4I1) were extracted and analyzed by PCR (**B**) and western blotting (**C**), respectively.

(**D**) HEK293T cells were cotransfected with Mito-GFP and pcDNA (Ctrl), CHDH + PARK2 or PINK1 + PARK2. Following treatment with DMSO or 100 μM CCCP for 2 h, the fluorescence of cells was measured, as described in the materials and methods. The signal of Mito-GFP in control extracts is fixed as 100 and the relative ratio to the control is indicated as the mean ± S.D. * $P < 0.05$.

Figure 3

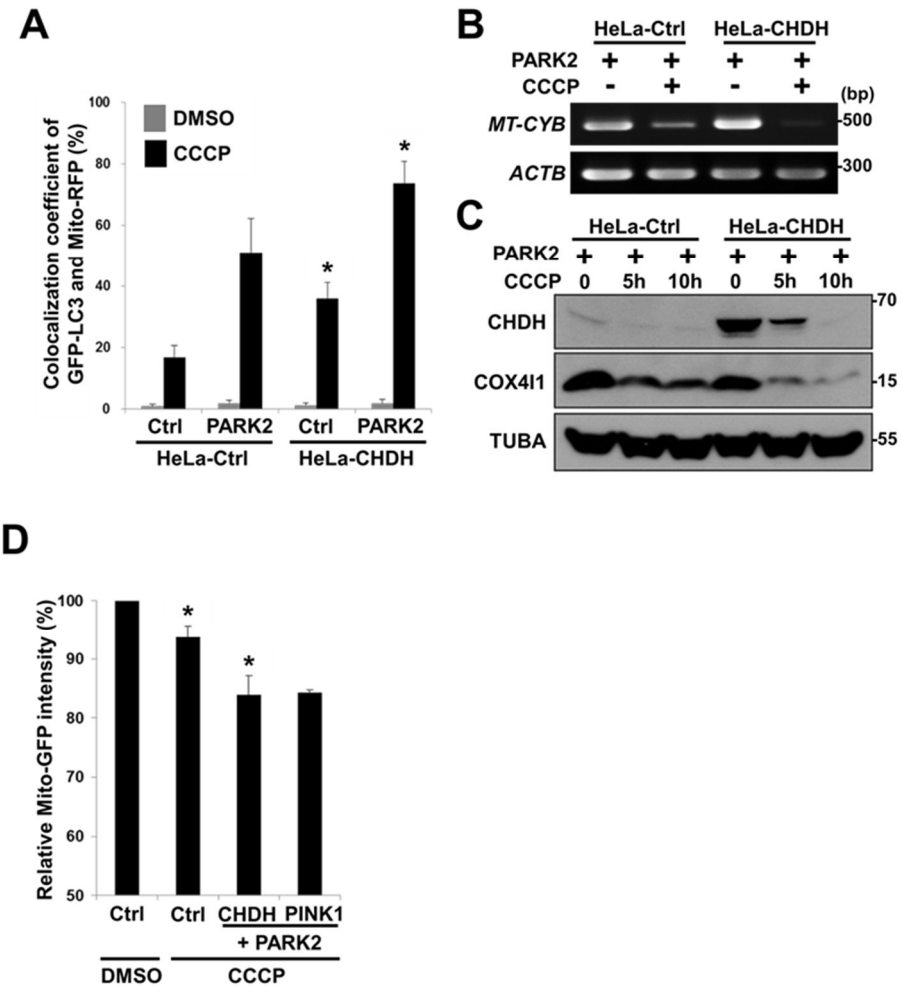
A
DMSO
CCCP
Colocalization coefficient of GFP-LC3 and Mito-RFP (%)
100
80
60
40
20
0
*
*
Ctrl
PARK2
Ctrl
PARK2
HeLa-Ctrl
HeLa-CHDH
B
HeLa-Ctrl
HeLa-CHDH
PARK2 + + + +
CCCP - + - +
(bp)
MT-CYB
500
ACTB
300
C
HeLa-Ctrl
HeLa-CHDH
PARK2 + + + + + +
CCCP 0 5h 10h 0 5h 10h
CHDH
70
COX4I1
15
TUBA
55
D
Relative Mito-GFP intensity (%)
100
90
80
70
60
50
*
*
Ctrl
Ctrl
CHDH PINK1
+ PARK2
DMSO
CCCP

**Figure 4. Effects of CHDH expression on PINK1-mediated mitophagy.**

(**A**) HeLa-Ctrl and HeLa-CHDH cells were cotransfected with PINK1-GFP and Mito-RFP and then exposed to 10 μM CCCP for 2 h, after which cells were examined under a confocal microscope.

(**B**) HeLa-control (Ctrl), CHDH overexpression (OE) and sh*CHDH* knockdown (KD) stable cells were exposed to 10 μM CCCP for 2 h. Cell extracts were analyzed with western blotting.

(**C**) SN4741 control (Ctrl) and PINK1 knockdown stable cells were transfected with CHDH, Mito-RFP and control GFP for 24 h and then left untreated or treated with 20 μM CCCP for 24 h. Mito-RFP-negative cells among total GFP-positive cells were counted under a fluorescence microscope. Bars represent the mean ± S.D. ($n > 3$).

## Figure 4

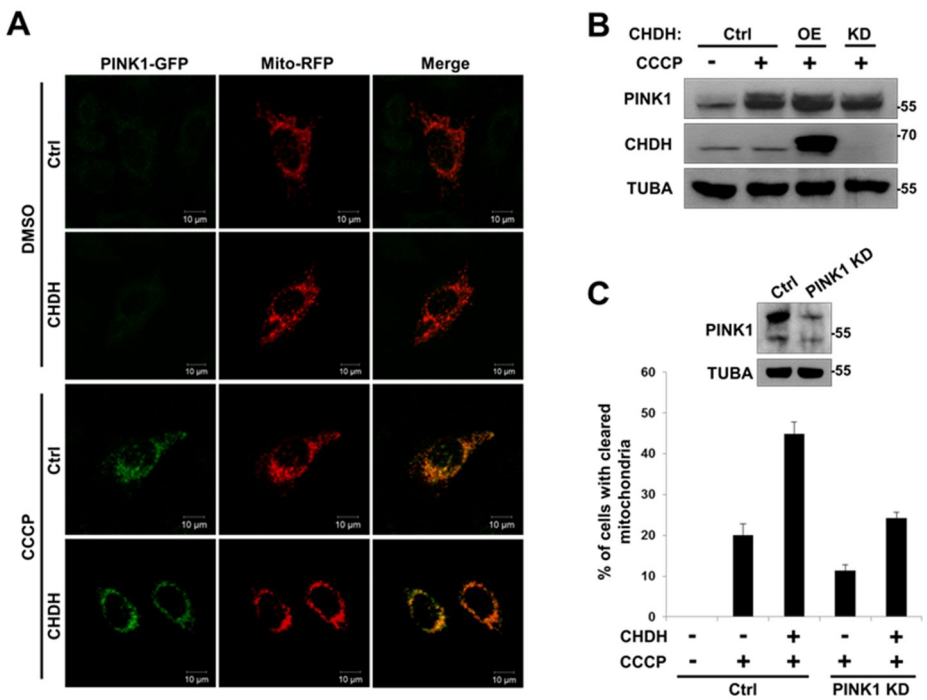
A
PINK1-GFP
Mito-RFP
Merge
DMSO
CCCP
Ctrl
CHDH
10 μm
B
CHDH:
Ctrl
OE
KD
CCCP
PINK1
CHDH
TUBA
55
70
55
C
Ctrl
PINK1 KD
PINK1
TUBA
55
55
% of cells with cleared mitochondria
60
50
40
30
20
10
0
CHDH
CCCP
Ctrl
PINK1 KD

**Figure 5. Schematic of CHDH full-length (FL) and deletion mutants (FB1Δ, RDΔ, and FB2Δ).**

**Figure 5**

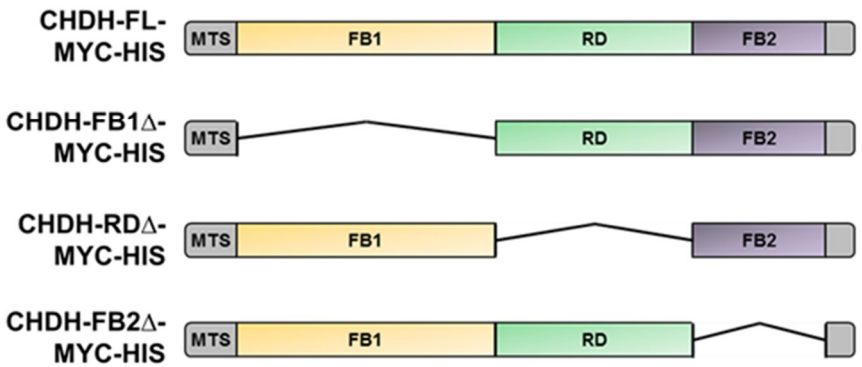
CHDH-FL-MYC-HIS
MTS
FB1
RD
FB2
CHDH-FB1Δ-MYC-HIS
MTS
RD
FB2
CHDH-RDΔ-MYC-HIS
MTS
FB1
FB2
CHDH-FB2Δ-MYC-HIS
MTS
FB1
RD

**Figure 6. Effects of CHDH deletion mutants on mitophagy.**

(**A**) HeLa cells were transfected with CHDH deletion mutants and then subjected to western blot analysis using MYC antibody.

(**B**) HeLa cells were transfected with GFP-LC3, Mito-RFP and either CHDH-FL or deletion mutants, and then analyzed under a confocal microscope at 4 h after treatment with 10 μM CCCP. Scale bar = 10 μM. TUBA, tubulin, alpha.

**Figure 6**

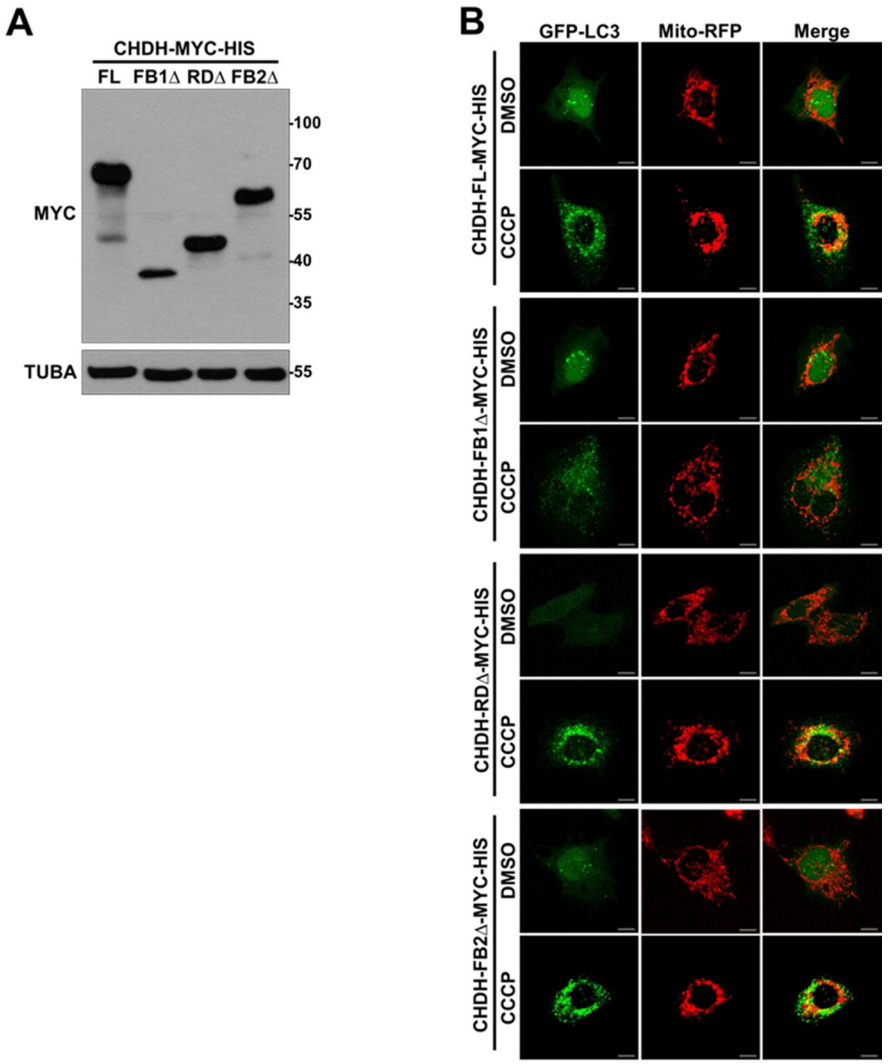
A
CHDH-MYC-HIS
FL FB1Δ RDΔ FB2Δ
MYC
TUBA
100
70
55
40
35
55
B
GFP-LC3
Mito-RFP
Merge
CHDH-FL-MYC-HIS
CHDH-FB1Δ-MYC-HIS
CHDH-RDΔ-MYC-HIS
CHDH-FB2Δ-MYC-HIS
DMSO
CCCP

**Figure 7. Mitophagic activity of CHDH is independent of its enzymatic activity.**

(**A**) The colocalization coefficient (%) of GFP-LC3 and Mito-RFP in the presence of CHDH-FL or deletion mutants was analyzed in the transfected cells under a confocal microscope and is represented as a bar graph with the mean ± S.D. Cells were treated with 10 μM CCCP for 4 h. * $P < 0.001$ ($n > 50$).

(**B**) HEK293T cells were transfected with CHDH or a series of deletion mutants and then subjected to LC-MS for measurement of enzyme activities, as described in the materials and methods.

**Figure 7**

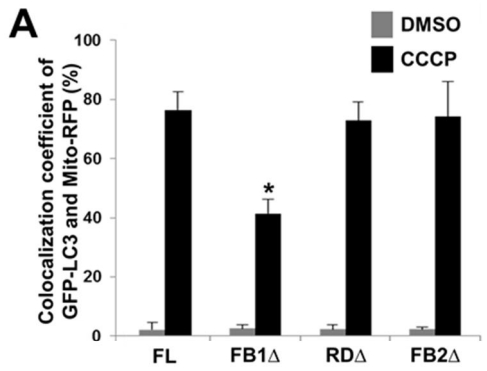
A
DMSO
CCCP
Colocalization coefficient of GFP-LC3 and Mito-RFP (%)
100
80
60
40
20
0
*
FL
FB1Δ
RDΔ
FB2Δ

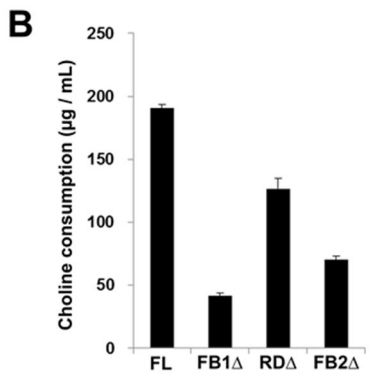
B
Choline consumption (μg / mL)
250
200
150
100
50
0
FL
FB1Δ
RDΔ
FB2Δ

**Figure 8. Betaine shows little effect on CHDH-mediated mitophagy.**

HeLa-Ctrl and HeLa-sh*CHDH* cells were cotransfected with PARK2, Mito-RFP and GFP-LC3 and then left untreated or exposed to 1 mM betaine for 2 h. After treatment with 20 μM CCCP for 2 h, cells were observed under a confocal microscope. The colocalization coefficient (%) between Mito-RFP and GFP-LC3 is represented as bars with the mean ± S.D. * $P < 0.001$ ($n > 50$).

**Figure 8**

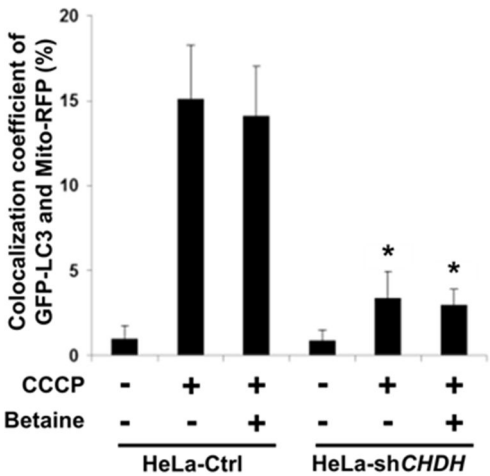
Colocalization coefficient of GFP-LC3 and Mito-RFP (%)
20
15
10
5
0
*
*
CCCP - + + - + +
Betaine - - + - - +
HeLa-Ctrl
HeLa-sh*CHDH*

**Figure 9. CHDH resides on the IM and OM of mitochondria.**

(**A**) HeLa cells were transfected with CHDH-MYC-HIS and Mito-RFP, followed by immunofluorescence analysis using MYC antibody (green) under a confocal microscope.

(**B**) HEK293T cells were subjected to submitochondrial fractionation analysis, as described in the materials and methods, and the fractions were verified using western blot analysis using the indicated antibodies.

(**C**) Mitochondria isolated from HeLa and HEK293T cells were treated with the increasing concentrations (0.25, 0.5, 0.75, 1, and 2 μg/mL) of proteinase K, and the reaction products were analyzed with western blotting.

Figure 9

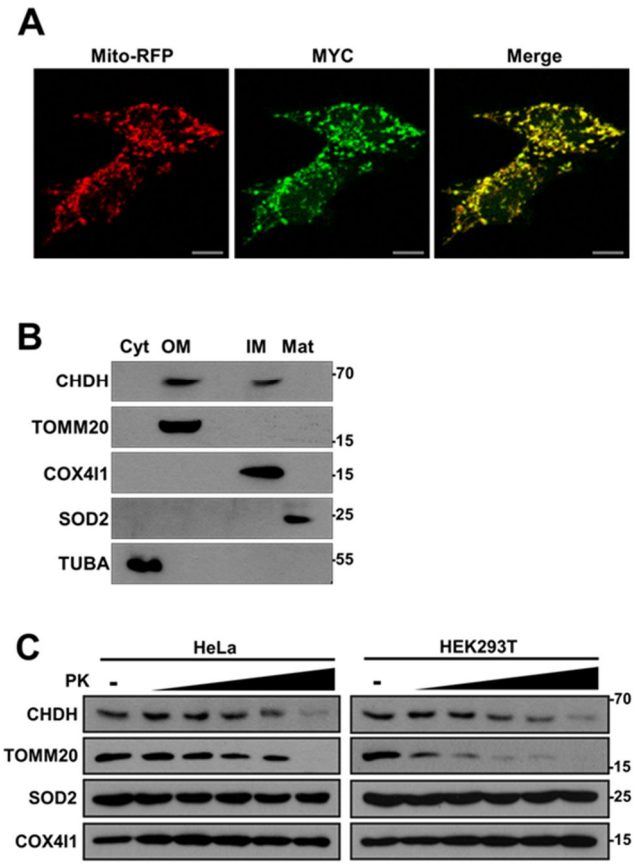
A
Mito-RFP
MYC
Merge
B
Cyt
OM
IM
Mat
CHDH
TOMM20
COX4I1
SOD2
TUBA
70
15
15
25
55
C
HeLa
HEK293T
PK
-
-
CHDH
TOMM20
SOD2
COX4I1
70
15
25
15

**Figure 10. Property of CHDH and effect of CCCP on mitochondrial membrane potential.**

(**A**) Pure mitochondria isolated from HEK293T cells were burst by sonication, incubated with Tris buffer (pH 8.0) containing 500 mM NaCl (left) or 1% Triton X-100 (right) for 30 min and then separated into the membrane-associated pellet (Pel) and soluble supernatant (Sup) fractions by ultracentrifugation. The fractions were analyzed by western blotting. Cytochrome c (CYCS) was used as a control of soluble proteins.

(**B**) HeLa cells were incubated with 100 nM TMRE for 20 min. After washing out the remaining dye with PBS, cells were treated for 30 min with the indicated concentrations of CCCP. Signal intensity of TMRE under a confocal microscope was measured using the ImageJ program and represented as bars with the mean ± S.D. ($n$ > 3).

Figure 10

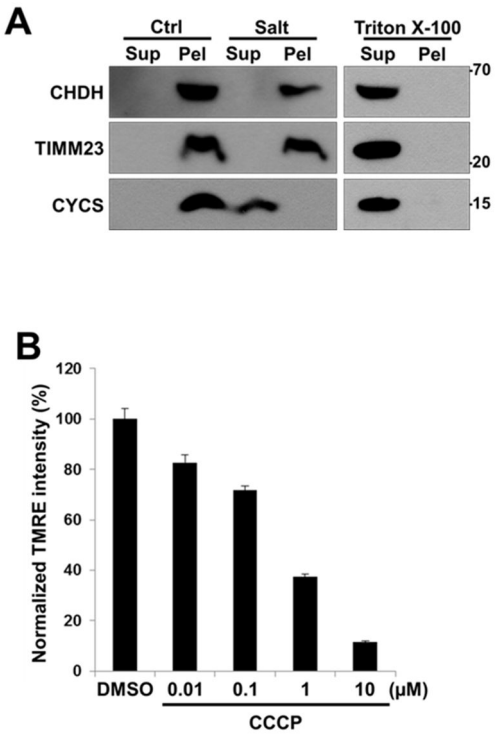
A
Ctrl
Salt
Triton X-100
Sup
Pel
Sup
Pel
Sup
Pel
CHDH
TIMM23
CYCS
70
20
15
B
Normalized TMRE intensity (%)
120
100
80
60
40
20
0
DMSO
0.01
0.1
1
10
(μM)
CCCP

**Figure 11. CHDH resides on the IM and OM of mitochondria and is enriched in the OM following CCCP treatment.**

(**A to C**) Following treatment of HEK293T cells with 0.1 μM CCCP for 30 min, mitochondria were purified and treated with Proteinase K (1 μg/mL), and the reaction products were analyzed using western blotting (**A**). HEK293T cells were pretreated with cycloheximide (CHX, 20 μg/mL) for 3 h and then exposed to 0.1 μM CCCP for 30 min, followed by submitochondrial fractionation and western blot analysis (**B**). The normalized relative ratio of CHDH signals detected in the OM and IM fractions on the blots in the (**B**) control group was determined by densitometric analysis using the ImageJ program (**C**).

**Figure 11**

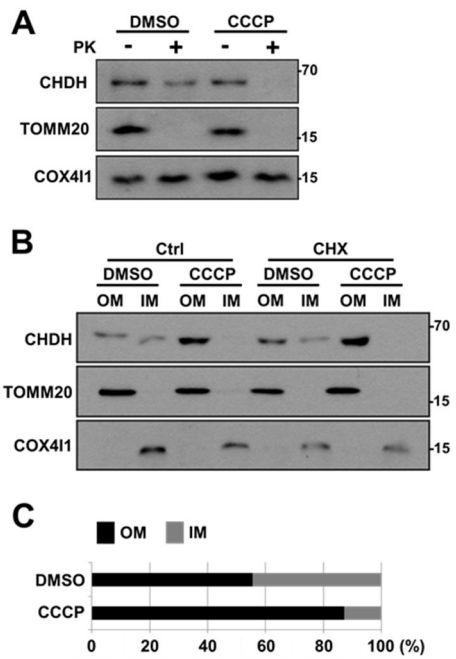
A
DMSO
CCCP
PK
-
+
-
+
CHDH
TOMM20
COX4I1
70
15
15
B
Ctrl
CHX
DMSO
CCCP
DMSO
CCCP
OM
IM
OM
IM
OM
IM
OM
IM
CHDH
TOMM20
COX4I1
70
15
15
C
OM
IM
DMSO
CCCP
0
20
40
60
80
100 (%)

**Figure 12. Topology of CHDH.**

(**A**) HeLa cells were transfected with HA-CHDH and treated with the annotated concentrations of CCCP for 30 min. Then, pure mitochondria were prepared and subjected to a proteinase K assay.

(**B**) HeLa cells were left untreated (Ctrl) or transfected with HA-CHDH-MYC-HIS. After permeabilization with 0.001% digitonin or 0.05% Triton X-100, cells were coimmunostained with TOMM20 (mouse/red) and SOD2 (rabbit/green) antibodies to confirm partial permeabilization (Ctrl) or with HA (mouse/red) and HIS (rabbit/green) antibodies (HA-CHDH-MYC-HIS) and then visualized under a confocal microscope. TUBA, tubulin, alpha.

(**C**) After treatment of SH-SY5Y cells with the increasing concentrations of CCCP (0.1 to 1 μM), mitochondria were purified, subjected to a proteinase K assay and analyzed by western blotting using CHDH antibody recognizing the C terminus. TUBA, tubulin, alpha.

Figure 12

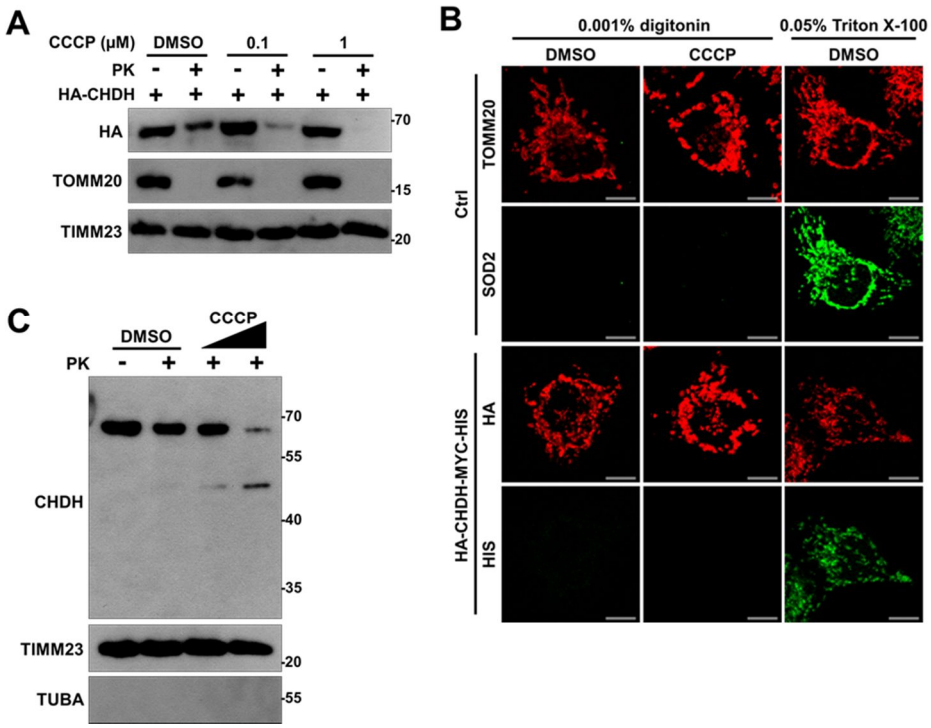
A
CCCP (μM)
DMSO
0.1
1
PK
HA-CHDH
HA
TOMM20
TIMM23
70
15
20
B
0.001% digitonin
0.05% Triton X-100
DMSO
CCCP
DMSO
Ctrl
TOMM20
SOD2
HA-CHDH-MYC-HIS
HA
HIS
C
DMSO
CCCP
PK
CHDH
TIMM23
TUBA
70
55
40
35
20
55

**Figure 13. Accumulation of CHDH on the mitochondrial outer membrane by HA-VDAC1.**

(**A**) HEK293T cells were transfected with HA-VDAC1 and treated with 1 μM CCCP for 30 min. Following immunoprecipitation (IP) with HA-antibody, the immunoprecipitates and whole cell lysates (WCL) were analyzed by western blotting.

(**B**) After treatment of HEK293T cells with 0.1 μM CCCP for 30 min, cell extracts were subjected to a proteinase K assay and then analyzed by western blotting.

(**C**) After transfection with PLSCR3, HEK293T cells were left untreated or treated with 0.1 μM CCCP for 30 min. Cell extracts were subjected to proteinase K assay and then analyzed by western blotting (left). The expression of PLSCR3 was confirmed by RT-PCR (right).

(**D**) SN4741-Ctrl and PINK1 knockdown cells were treated with 10 μM CCCP for 2 h and cell extracts were then analyzed by western blotting. TUBA, tubulin, alpha.

**Figure 13**

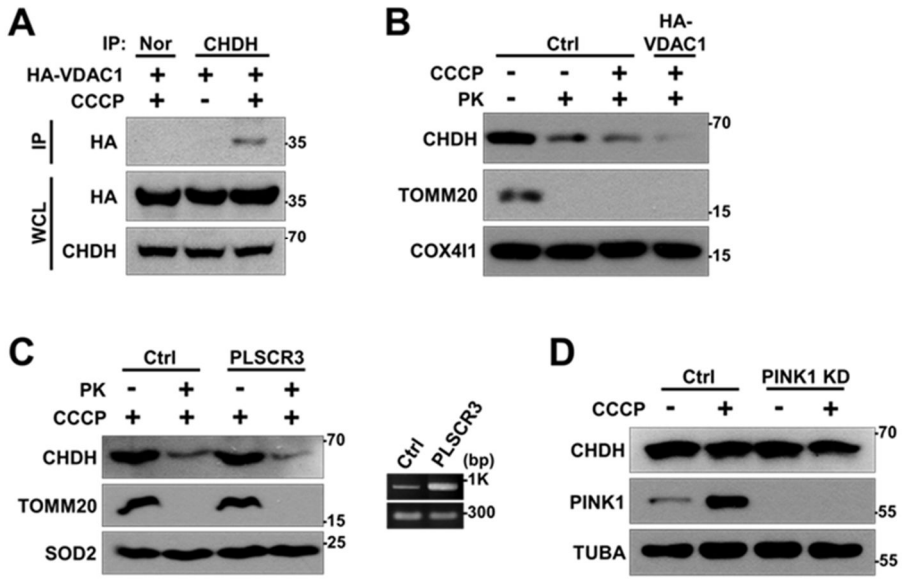
A
IP: Nor CHDH
HA-VDAC1 + + +
CCCP + - +
IP
HA
35
WCL
HA
35
CHDH
70
B
Ctrl
HA-VDAC1
CCCP - - + +
PK - + + +
CHDH
70
TOMM20
15
COX4I1
15
C
Ctrl
PLSCR3
PK - + - +
CCCP + + + +
CHDH
70
TOMM20
15
SOD2
25
Ctrl
PLSCR3
(bp)
1K
300
D
Ctrl
PINK1 KD
CCCP - + - +
CHDH
70
PINK1
55
TUBA
55

**Figure 14. CHDH binds to SQSTM1.**

(**A**) HEK293T cells were transfected with pcDNA (Ctrl) or HA-CHDH and then left untreated or treated with 10 μM CCCP for 30 min. Cell extracts were prepared and subjected to immunoprecipitation (IP) analysis using a CHDH antibody. The immunoprecipitates and whole cell lysates (WCL) were analyzed by western blotting. (**B and C**) SH-SY5Y cells were treated with 20 μM CCCP for the indicated times (**B**) or for 30 min (**C**). Cell extracts were subjected to immunoprecipitation (IP) analysis using preimmune normal (Nor) and CHDH antibody (**B**) or SQSTM1 antibody (**C**). TOMM20, COX4I1 and SOD2 were used as negative controls in western blotting (**B**).

Figure 14

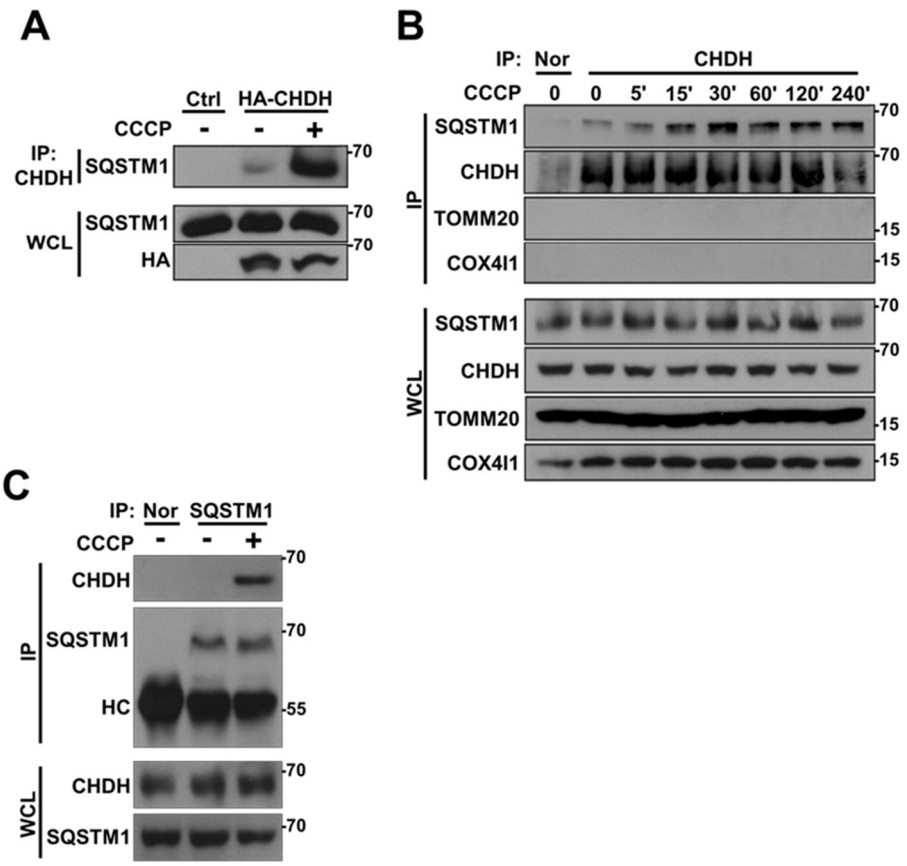
A
Ctrl
HA-CHDH
CCCP
-
-
+
IP: CHDH
SQSTM1
70
WCL
SQSTM1
70
HA
70
B
IP: Nor
CHDH
CCCP
0
0
5'
15'
30'
60'
120'
240'
IP
SQSTM1
70
CHDH
70
TOMM20
15
COX4I1
15
WCL
SQSTM1
70
CHDH
70
TOMM20
15
COX4I1
15
C
IP: Nor
SQSTM1
CCCP
-
-
+
IP
CHDH
70
SQSTM1
70
HC
55
WCL
CHDH
70
SQSTM1
70

**Figure 15. Interaction between CHDH and SQSTM1.**

(**A**) HeLa-Ctrl and HeLa-sh*CHDH* cells were left untreated or treated with 10 μM CCCP for 5 h and cell extracts were subjected to immunoprecipitation (IP) analysis using CHDH antibody.

(**B**) HeLa-Ctrl and HeLa-sh*CHDH* cells were transfected with FLAG-Ctrl or FLAG-PARK2 and then left untreated or exposed to 20 μM CCCP for 30 min. Cell extracts were subjected to immunoprecipitation (IP) analysis using a CHDH antibody. The asterisk indicates a heavy chain that is weakly bound across species.

(**C**) HeLa cells were transfected with HA-VDAC1, CHDH and either control vector or PARK2 as indicated, and then treated with 10 μM CCCP for 3 h in the presence or absence of 5 μM MG132 or 20 nM bafilomycin $A_1$ (Baf).

Figure 15

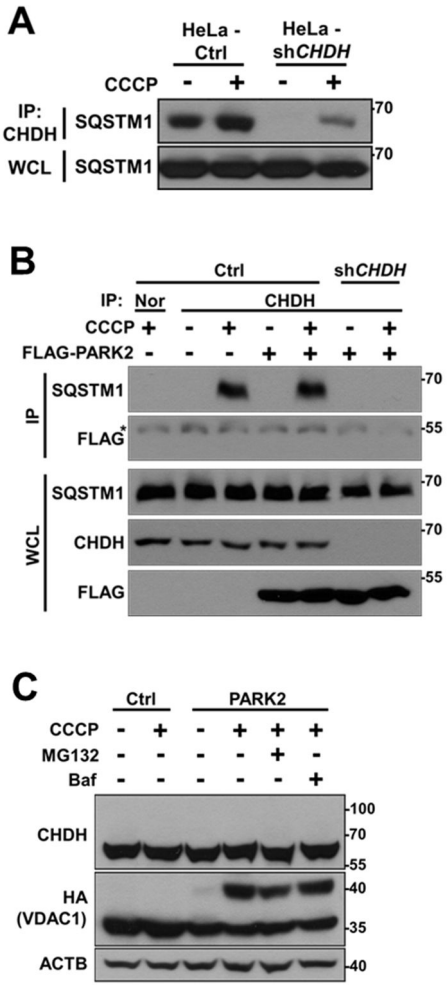
A
HeLa - Ctrl
HeLa - shCHDH
CCCP - + - +
IP: CHDH | SQSTM1
WCL | SQSTM1
70
70
B
Ctrl
shCHDH
IP: Nor
CHDH
CCCP + - + - + - +
FLAG-PARK2 - - - + + + +
IP
SQSTM1
FLAG*
WCL
SQSTM1
CHDH
FLAG
70
55
70
70
55
C
Ctrl
PARK2
CCCP - + - + + +
MG132 - - - - + -
Baf - - - - - +
CHDH
HA (VDAC1)
ACTB
100
70
55
40
35
40

**Figure 16. CHDH binds to SQSTM1, which requires the CHDH FB1 and SQSTM1 PB1 domains.**

(**A**) A schematic representation of SQSTM1 full-length (FL) and the PB1-deletion mutant (PB1Δ).

(**B, C**) HEK293T cells were transfected with SQSTM1-FL-MYC-HIS or SQSTM1-PB1Δ-MYC-HIS and then treated with 20 μM CCCP for 30 min, after which cell lysates were subjected to immunoprecipitation (IP) analysis using CHDH antibody (**B**, upper) or MYC antibody (**C**, upper). The immunoprecipitates and whole cell lysates (WCL) were analyzed by western blotting (lower).

(**D**) HEK293T cells were transfected with CHDH-MYC and its deletion mutants and then treated with 10 μM CCCP for 30 min, after which cell lysates were subjected to IP analysis using a MYC antibody.

Figure 16

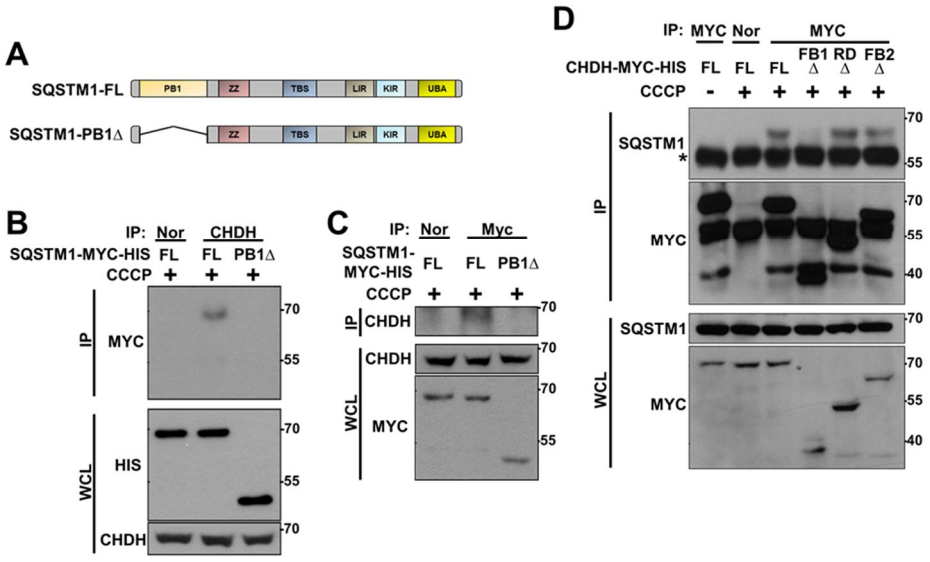
A
SQSTM1-FL
PB1
ZZ
TBS
LIR
KIR
UBA
SQSTM1-PB1Δ
B
IP: Nor CHDH
SQSTM1-MYC-HIS FL FL PB1Δ
CCCP + + +
IP
MYC
WCL
HIS
CHDH
70
55
C
IP: Nor Myc
SQSTM1-MYC-HIS FL FL PB1Δ
CCCP + + +
IP
CHDH
WCL
CHDH
MYC
70
55
40
D
IP: MYC Nor MYC
CHDH-MYC-HIS FL FL FL FB1Δ RDΔ FB2Δ
CCCP - + + + + +
IP
SQSTM1*
MYC
WCL
SQSTM1
MYC
70
55
40

**Figure 17. CHDH- FB1Δ on mitophagy.**

(**A**) HeLa cells were transfected with CHDH-FL-MYC-HIS or CHDH-FB1Δ-MYC-HIS and then exposed to 20 μM CCCP for 3 h. Cells were examined with immunofluorescence analysis using MYC and SQSTM1 antibodies. Scale bar = 10 μM. Enlarged sections are shown on right side with labelling (a to d).

(**B**) HeLa cells were transfected with HA-VDAC1, PARK2 and either CHDH-FL or FB1Δ for 24 h and incubated with 20 μM CCCP for 2 h. Cell extracts were analyzed by western blotting.

(**C**) HEK293T cells were transfected with CHDH wild-type (WT) or rs12676 SNP containing CHDH-R78L and then incubated with 20 μM CCCP for 30 min. Samples were immunoprecipitated (IP) with preimmune normal (Nor) or CHDH antibody followed by western blot analysis.

Figure 17

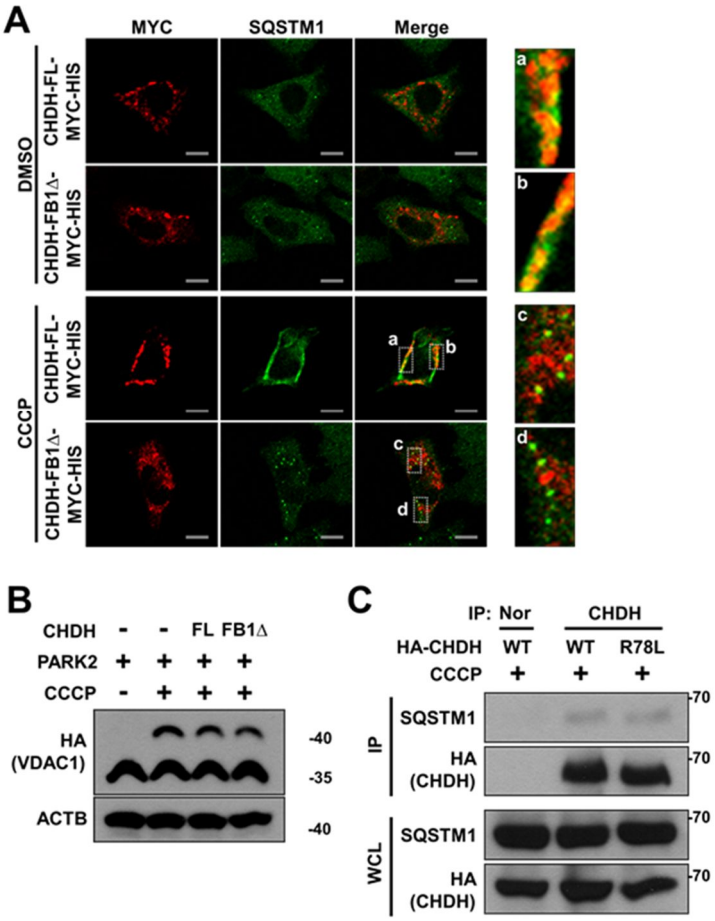
A
MYC
SQSTM1
Merge
DMSO
CHDH-FL-MYC-HIS
CHDH-FB1Δ-MYC-HIS
CCCP
CHDH-FL-MYC-HIS
CHDH-FB1Δ-MYC-HIS
a
b
c
d
B
CHDH - - FL FB1Δ
PARK2 + + + +
CCCP - + + +
HA (VDAC1)
ACTB
-40
-35
-40
C
IP: Nor CHDH
HA-CHDH WT WT R78L
CCCP + + +
IP
SQSTM1
HA (CHDH)
WCL
SQSTM1
HA (CHDH)
70
70
70
70

**Figure 18. CHDH recruits SQSTM1 onto mitochondria during mitophagy.**

(**A, B**) HeLa-Ctrl and HeLa-sh*CHDH* cells were transfected with Mito-RFP and FLAG-PARK2 and treated with 10 μM CCCP for 4 h. Following immunostaining with a SQSTM1 antibody, cells were examined under a confocal microscope (**A**) and the colocalization coefficient (%) of SQSTM1 and Mito-RFP was determined. Bars represent the mean ± S.D. * $P < 0.0001$ ($n > 50$) (**B**).

Figure 18

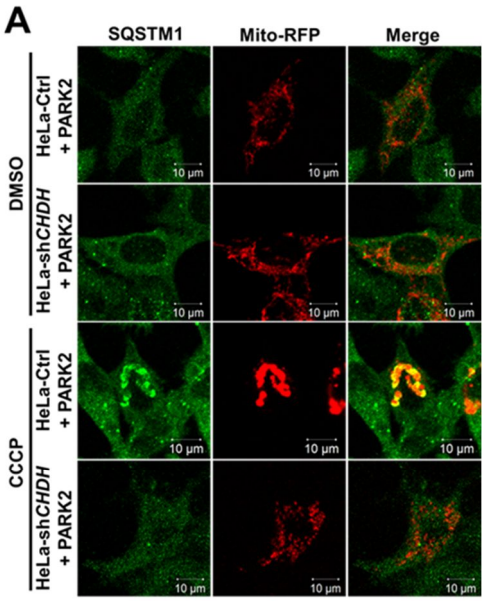
A
SQSTM1
Mito-RFP
Merge
DMSO
HeLa-Ctrl + PARK2
HeLa-shCHDH + PARK2
CCCP
HeLa-Ctrl + PARK2
HeLa-shCHDH + PARK2
10 μm

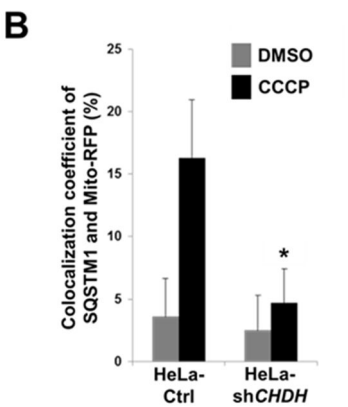
B
DMSO
CCCP
Colocalization coefficient of SQSTM1 and Mito-RFP (%)
25
20
15
10
5
0
*
HeLa-Ctrl
HeLa-shCHDH

**Figure 19. CHDH recruits SQSTM1 onto mitochondria during mitophagy.**

(**A**) SH-SY5Y-Ctrl and SH-SY5Y-sh*CHDH* stable cells were treated with 20 μM CCCP for the indicated times and mitochondria were purified and analyzed by western blotting using the indicated antibodies.

(**B**) HEK293T cells were transfected with CHDH-FL or CHDH-FB1Δ and then treated with 10 μM CCCP for the indicated times. Cell extracts were fractionated to isolate mitochondria followed by western blot analysis.

(**C**) HEK293T cells were transfected with scrambled siRNA (Scr) or *SQSTM1* siRNA for 48 h. After treatment with 10 μM CCCP for 24 h, cell extracts were prepared and subjected to western blot analysis.

**Figure 19**

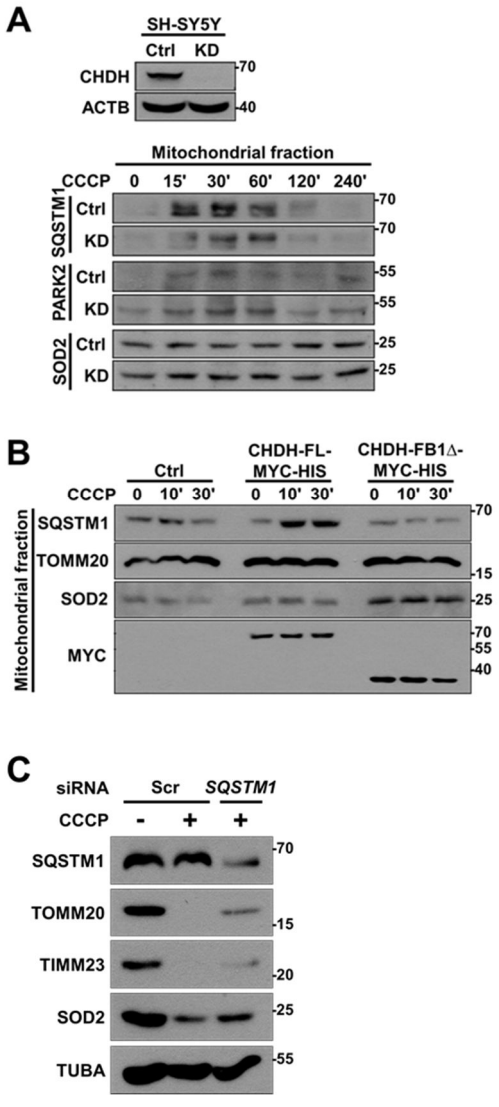
A
SH-SY5Y
Ctrl KD
CHDH
ACTB
70
40
Mitochondrial fraction
CCCP 0 15' 30' 60' 120' 240'
SQSTM1 Ctrl
KD
PARK2 Ctrl
KD
SOD2 Ctrl
KD
70
70
55
55
25
25
B
Ctrl
CHDH-FL-MYC-HIS
CHDH-FB1Δ-MYC-HIS
CCCP 0 10' 30' 0 10' 30' 0 10' 30'
Mitochondrial fraction
SQSTM1
TOMM20
SOD2
MYC
70
15
25
70
55
40
C
siRNA Scr SQSTM1
CCCP - + +
SQSTM1
TOMM20
TIMM23
SOD2
TUBA
70
15
20
25
55

**Figure 20. Interaction of CHDH with SQSTM1 increases the recruitment of LC3 into mitochondria to process mitophagy.**

(**A**) HeLa-Ctrl and HeLa-sh*CHDH* cells were cotransfected with GFP-LC3, Mito-RFP and either control vector (Ctrl) or PARK2. Following treatment with DMSO or 10 μM CCCP for 4 h, cells were fixed and observed under a confocal microscope. The colocalization coefficient (%) of GFP-LC3 and Mito-RFP was determined and bars represent the mean ± S.D. * $P < 0.005$ ($n > 50$).

(**B**) After HeLa cells were transfected with CHDH-FL-MYC-HIS or CHDH-FB1Δ-MYC-HIS and treated with 10 μM CCCP for 30 min, samples were subjected to an immunoprecipitation (IP) assay using preimmune (Nor) or a MYC antibody. The asterisk indicates the heavy chain of the MYC antibody.

(**C**) *sqstm1* KO MEF cells were exposed to 10 μM CCCP for 30 min. Cell extracts were subjected to an immunoprecipitation (IP) assay using a CHDH antibody and the immunoprecipitates and whole cell lysates (WCL) were analyzed by western blot.

(**D**) HeLa cells were cotransfected with PARK2-GFP and either CHDH or CHDH-

FB1Δ, treated with 10 μM CCCP for 24 h and then immunostained with a TOMM20 antibody. The percentage of cells showing reduced immunoreactivity against TOMM20 was determined using a confocal microscope and is represented as bars ± S.D. * $P < 0.001$ ($n > 50$).

**Figure 20**

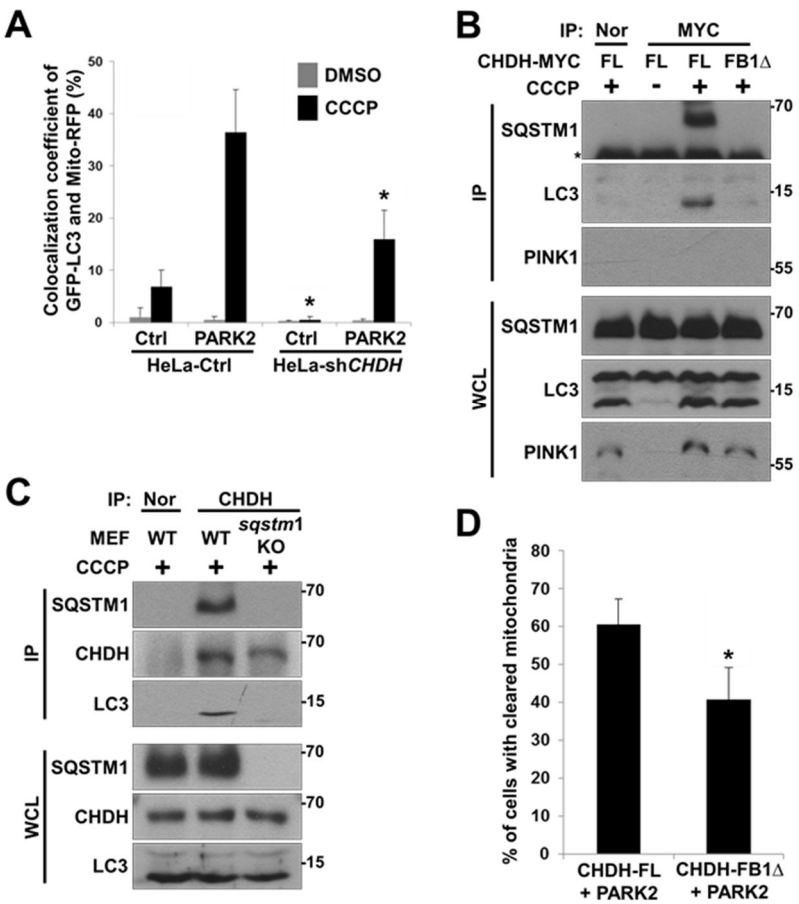
A
Colocalization coefficient of GFP-LC3 and Mito-RFP (%)
DMSO
CCCP
Ctrl
PARK2
Ctrl
PARK2
HeLa-Ctrl
HeLa-shCHDH
B
IP: Nor MYC
CHDH-MYC FL FL FL FB1Δ
CCCP + - + +
IP
SQSTM1
LC3
PINK1
WCL
SQSTM1
LC3
PINK1
C
IP: Nor CHDH
MEF WT WT sqstm1 KO
CCCP + + +
IP
SQSTM1
CHDH
LC3
WCL
SQSTM1
CHDH
LC3
D
% of cells with cleared mitochondria
CHDH-FL + PARK2
CHDH-FB1Δ + PARK2

**Figure 21. Mitochondrial targetting of FB1 domain enhances mitophagy.**

(**A**) Schematic diagram of TOMM20-FB1-GFP chimera (upper). HeLa cells were transfected with mRFP-LC3 and either TOMM20-GFP or TOMM20-FB1-GFP and exposed to 10 μM CCCP for 1 h. Cells were analyzed under a confocal microscope and the colocalization coefficient was determined. Bars represent the mean ± S.D. * $P < 0.0001$ (lower) ($n > 50$).

(**B**) HEK293T cells were transfected with different concentrations of GFP (Ctrl-GFP) or FB1-GFP (+: 2 μg, ++: 5 μg) and then treated with 10 μM CCCP for 30 min. Cell lysates were analyzed by immunoprecipitation (IP) and western blotting.

Figure 21

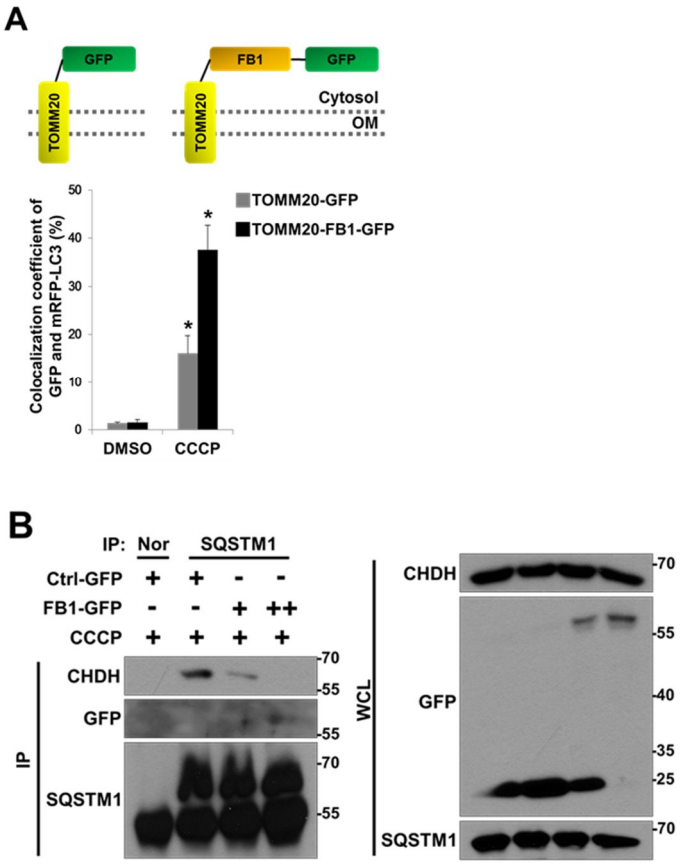
A
GFP
TOMM20
FB1
GFP
TOMM20
Cytosol
OM
TOMM20-GFP
TOMM20-FB1-GFP
Colocalization coefficient of GFP and mRFP-LC3 (%)
50
40
30
20
10
0
*
*
DMSO
CCCP
B
IP: Nor SQSTM1
Ctrl-GFP + + - -
FB1-GFP - - + ++
CCCP + + + +
IP
CHDH
GFP
SQSTM1
70
55
55
70
55
WCL
CHDH
GFP
SQSTM1
70
55
40
35
25
70

**Figure 22. Inhibition of the interaction between CHDH and SQSTM1 hampers mitochondrial degradation.**

(**A, B**) HeLa cells were transfected with PARK2 and either Ctrl-GFP or FB1-GFP. Following 24 h treatment with 10 μM CCCP, cells were subjected to immunocytochemical analysis using the indicated antibodies and then visualized under a confocal microscope. Scale bar = 10 μM. Statistical values for (**A**) are represented as bars with the mean ± S.D. * $P < 0.05$ (**B**) ($n > 50$).

(**C**) HeLa cells were transfected with FB1-GFP and SQSTM1-MYC-HIS. After treatment with 10 μM CCCP for 24 h, cells were immunostained with MYC antibody and then observed under a confocal microscope. Scale bar = 10 μM. TUBA, tubulin, alpha.

(**D**) Stable SN4741-Ctrl or SN4741-sh*CHDH* cells were transfected with GFP-LC3 and Mito-RFP and then treated with 100 μM MPP+ for 4 h. Cells were examined under a confocal microscope. The expression level of CHDH was determined using western blot analysis (upper) and the colocalization coefficient (%) between GFP-LC3

and Mito-RFP was determined (lower). Bars represent the mean ± S.D. * $P < 0.0001$ ($n > 50$).

Figure 22

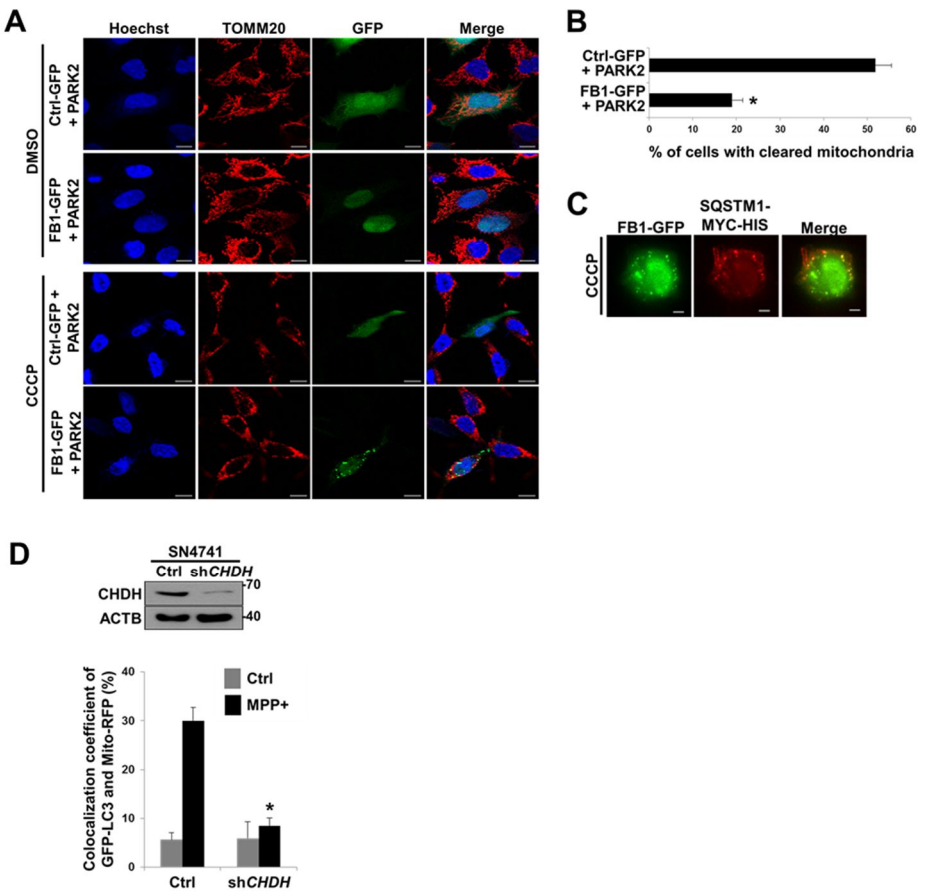
A
Hoechst
TOMM20
GFP
Merge
DMSO
Ctrl-GFP + PARK2
FB1-GFP + PARK2
CCCP
Ctrl-GFP + PARK2
FB1-GFP + PARK2
B
Ctrl-GFP + PARK2
FB1-GFP + PARK2
*
0
10
20
30
40
50
60
% of cells with cleared mitochondria
C
SQSTM1-MYC-HIS
FB1-GFP
Merge
CCCP
D
SN4741
Ctrl
shCHDH
CHDH
ACTB
70
40
Colocalization coefficient of GFP-LC3 and Mito-RFP (%)
Ctrl
MPP+
*
0
10
20
30
40
Ctrl
shCHDH

**Figure 23. Proposed role of CHDH in mitophagy.**

CHDH resides on both the OM and IM of mitochondria and exposes its FB1 domain-containing N terminus to the cytosol on the OM. Following mitochondrial depolarization, CHDH accumulates on the OM probably through VDAC1 and interacts with SQSTM1 to recruit LC3 to the damaged mitochondria for mitophagy.

Figure 23

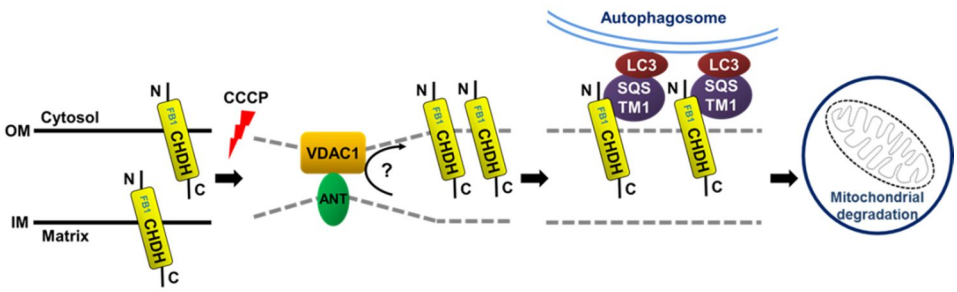
Autophagosome
LC3
SQS
TM1
N
C
FB1
CHDH
CCCP
OM
Cytosol
IM
Matrix
VDAC1
ANT
?
Mitochondrial
degradation

# 4. DISCUSSION

Although CHDH has been proposed to localize to the IM of mitochondria,[1, 32, 33] it is surprising to note that no report has clearly demonstrated the presence of CHDH in the IM of mitochondria. My results indicate that CHDH resides on both the OM and IM of mitochondria. More interestingly, CHDH accumulates on the OM during mitochondrial depolarization. Thus, it appears that CHDH plays a dual role in choline conversion and mitophagy in the IM and OM, respectively, of mitochondria. Concordant with this hypothesis, I found no correlation between the enzymatic activity and mitophagic function of CHDH, in that enzyme activity-dead mutant of CHDH were functional in mitophagy and the CHDH FB1 domain was crucial only for mitophagy. In addition, my observation that betaine, the enzymatic product of CHDH, cannot rescue the impaired mitophagy caused by CHDH deficiency further distinguishes CHDH's mitophagic activity from its enzymatic activity.

Given this newly discovered role in mitophagy, the location of CHDH within

mitochondria becomes more important. PINK1 also resides on both the OM and IM of mitochondria, and is likewise involved in mitophagy. Although PINK1 is normally degraded in the IM of mitochondria following cleavage by PARL proteases,[19] it accumulates on the mitochondrial surface to recruit PARK2 during mitophagy.[20, 42] In contrast to PINK1, however, western blot analysis did not show any cleavage or posttranslational modification, such as ubiquitination, of CHDH during mitophagy, suggesting that the accumulation of CHDH on the OM may not be accompanied by such modifications. Cardiolipin, a phospholipid located on the mitochondrial IM, is externalized to the OM by PLSCR3 following mitochondrial injury, where it interacts with LC3.[35] However, I observed no significant effect of PLSCR3 on the accumulation of CHDH in the OM. Instead, I found that the accumulation of CHDH on the OM depends on the mitochondrial potential and may use the VDAC1-containing mitochondrial membrane contact site as a path.

It appears that the accumulation of CHDH on the OM of depolarized mitochondria is critical to facilitate interaction with cytosolic SQSTM1. In particular,

the CHDH N-terminal region, which is approximately 20 kDa in size and exposed to the cytosol in the FB1 domain, seems to be important for this interaction. Although the CHDH FB1 domain is required for this interaction and ectopic expression of the CHDH FB1 domain interrupts the interaction of CHDH with SQSTM1, it remains unclear whether the CHDH FB1 domain alone is sufficient to recruit SQSTM1 onto damaged mitochondria. By BLAST search, I found that there was no significant FB1 domain-containing protein in human proteome. My observation that TOMM20-FB1-GFP functioned in recruiting LC3 to depolarized mitochondria in the presence of CCCP does not exclude a mechanism in which other mitophagic component(s) or machinery, such as PARK2 substrates, operate in parallel during mitophagy, in addition to the presence of CHDH on the OM.

Although the ubiquitination of mitochondrial substrates by PARK2 is also crucial to recruit SQSTM1 into impaired mitochondria,[26, 43, 44] it has previously been reported that SQSTM1 interacts with non-ubiquitinated substrates via its PB1 domain.[38, 39] The PB1 domain is responsible for forming SQSTM1 aggregates through self- or hetero-

oligomerization[45, 46] and is required for mitochondrial aggregation and localization of SQSTM1 to mitochondria during CCCP conditions.[44] Here, I elucidate the mechanism by which SQSTM1 may be recruited into impaired mitochondria, involving an interaction between SQSTM1 and non-ubiquitinated CHDH on the OM of mitochondria. Although I observed some interaction of SQSTM1 with CHDH at the steady-state level required for basal mitophagy, the interaction drastically increased upon mitophagy induction. Despite some debate on the necessity and sufficiency of SQSTM1 in mitochondrial clearance,[11, 26, 44, 47] the results from my assays show that SQSTM1 is necessary for the degradation of depolarized mitochondria. It remains possible that SQSTM1 and other adaptor proteins may work together in mitophagy. While SQSTM1 is crucial in mediating mitophagy in several cell lines, it does not act alone, because knockdown of CHDH expression suppressed CCCP-induced LC3 recruitment into the mitochondria by just over 50%, despite complete inhibition of the colocalization of SQSTM1 with mitochondria. Thus, in the absence of SQSTM1, other adaptors, such as HDAC6, may compensate for SQSTM1 deficiency.[43, 48]

The effect of CHDH on mitophagy was displayed largely with PINK1 and PARK2. In the absence of PINK1 and PARK2, however, CHDH overexpression could still stimulate mitophagy, while absolute levels of mitophagy were reduced. Similarly, PARK2-mediated mitophagy was significantly impaired in the absence of CHDH. The function of CHDH appears to be independent of PINK1 and PARK2, since neither the recruitment of PARK2 to depolarized mitochondria nor the stabilization of PINK1 was affected by CHDH. Further, CHDH is apparently not a substrate of PARK2 and its interaction with SQSTM1 is PARK2-independent. My current hypothesis is that CHDH functions in parallel with PINK1/PARK2 pathway in mitophagy. Thus, CHDH is also important for the recruitment of LC3 into mitochondria in PARK2-mediated mitophagy. In addition to PINK1 and PARK2, BNIP3L/NIX and FUNDC1 have recently been reported to function in hypoxial mitophagy.[49, 50] While it seems that CHDH may not function during hypoxial mitophagy (data not shown), I now add CHDH to the list of mitophagy coordinators. In conclusion, CHDH accumulates on the OM of mitochondria following mitochondrial damage and interacts there with

SQSTM1 to recruit LC3 into the impaired mitochondria for mitophagic clearance (**Fig. 23**). This mitophagic function of CHDH is independent of its conventional enzymatic activity but is necessary for PARK2-mediated mitophagy. Finally, the implications of CHDH malfunction in mitophagy-associated pathology are now widely open and remain to be further addressed.

# 5. REFERENCES

1. De Ridder JJ, van Dam K. The efflux of betaine from rat-liver mitochondria, a possible regulating step in choline oxidation. Biochim Biophys Acta 1973; 291:557-63.

2. Garrow TA. Purification, kinetic properties, and cDNA cloning of mammalian betaine-homocysteine methyltransferase. J Biol Chem 1996; 271:22831-8.

3. Olthof MR, Verhoef P. Effects of betaine intake on plasma homocysteine concentrations and consequences for health. Curr Drug Metab 2005; 6:15-22.

4. Ma XJ, Wang Z, Ryan PD, Isakoff SJ, Barmettler A, Fuller A, Muir B, Mohapatra G, Salunga R, Tuggle JT, et al. A two-gene expression ratio predicts clinical outcome in breast cancer patients treated with tamoxifen. Cancer Cell 2004;

5:607-16.

5. Wang Z, Dahiya S, Provencher H, Muir B, Carney E, Coser K, Shioda T, Ma XJ, Sgroi DC. The prognostic biomarkers HOXB13, IL17BR, and CHDH are regulated by estrogen in breast cancer. Clin Cancer Res 2007; 13:6327-34.

6. Johnson AR, Craciunescu CN, Guo Z, Teng YW, Thresher RJ, Blusztajn JK, Zeisel SH. Deletion of murine choline dehydrogenase results in diminished sperm motility. FASEB J 2010; 24:2752-61.

7. da Costa KA, Kozyreva OG, Song J, Galanko JA, Fischer LM, Zeisel SH. Common genetic polymorphisms affect the human requirement for the nutrient choline. FASEB J 2006; 20:1336-44.

8. Xu X, Gammon MD, Zeisel SH, Lee YL, Wetmur JG, Teitelbaum SL,

Bradshaw PT, Neugut AI, Santella RM, Chen J. Choline metabolism and risk of breast cancer in a population-based study. FASEB J 2008; 22:2045-52.

9. Johnson AR, Lao S, Wang T, Galanko JA, Zeisel SH. Choline dehydrogenase polymorphism rs12676 is a functional variation and is associated with changes in human sperm cell function. PLoS One 2012; 7:e36047.

10. Tatsuta T, Langer T. Quality control of mitochondria: protection against neurodegeneration and ageing. EMBO J 2008; 27:306-14.

11. Ding WX, Ni HM, Li M, Liao Y, Chen XY, Stolz DB, Dorn GW, Yin XM. Nix Is Critical to Two Distinct Phases of Mitophagy, Reactive Oxygen Species-mediated Autophagy Induction and Parkin-Ubiquitin-p62-mediated Mitochondrial Priming. J Biol Chem 2010; 285:27879-90.

12. Itakura E, Kishi-Itakura C, Koyama-Honda I, Mizushima N. Structures containing Atg9A and the ULK1 complex independently target depolarized mitochondria at initial stages of Parkin-mediated mitophagy. J Cell Sci 2012; 125:1488-99.

13. Joo JH, Dorsey FC, Joshi A, Hennessy-Walters KM, Rose KL, McCastlain K, Zhang J, Iyengar R, Jung CH, Suen DF, et al. Hsp90-Cdc37 chaperone complex regulates Ulk1- and Atg13-mediated mitophagy. Mol Cell 2011; 43:572-85.

14. Ashrafi G, Schwarz TL. The pathways of mitophagy for quality control and clearance of mitochondria. Cell Death Differ 2012.

15. Chu CT, Zhu J, Dagda R. Beclin 1-independent pathway of damage-induced mitophagy and autophagic stress: implications for neurodegeneration and cell death. Autophagy 2007; 3:663-6.

16. Gilkerson RW, De Vries RL, Lebot P, Wikstrom JD, Torgyekes E, Shirihai OS, Przedborski S, Schon EA. Mitochondrial autophagy in cells with mtDNA mutations results from synergistic loss of transmembrane potential and mTORC1 inhibition. Hum Mol Genet 2012; 21:978-90.

17. Kitada T, Asakawa S, Hattori N, Matsumine H, Yamamura Y, Minoshima S, Yokochi M, Mizuno Y, Shimizu N. Mutations in the parkin gene cause autosomal recessive juvenile parkinsonism. Nature 1998; 392:605-8.

18. Valente EM, Abou-Sleiman PM, Caputo V, Muqit MM, Harvey K, Gispert S, Ali Z, Del Turco D, Bentivoglio AR, Healy DG, et al. Hereditary early-onset Parkinson's disease caused by mutations in PINK1. Science 2004; 304:1158-60.

19. Greene AW, Grenier K, Aguileta MA, Muise S, Farazifard R, Haque ME,

McBride HM, Park DS, Fon EA. Mitochondrial processing peptidase regulates PINK1 processing, import and Parkin recruitment. EMBO Rep 2012; 13:378-85.

20. Jin SM, Lazarou M, Wang C, Kane LA, Narendra DP, Youle RJ. Mitochondrial membrane potential regulates PINK1 import and proteolytic destabilization by PARL. J Cell Biol 2010; 191:933-42.

21. Matsuda N, Sato S, Shiba K, Okatsu K, Saisho K, Gautier CA, Sou YS, Saiki S, Kawajiri S, Sato F, et al. PINK1 stabilized by mitochondrial depolarization recruits Parkin to damaged mitochondria and activates latent Parkin for mitophagy. J Cell Biol 2010; 189:211-21.

22. Kanki T, Wang K, Cao Y, Baba M, Klionsky DJ. Atg32 is a mitochondrial protein that confers selectivity during mitophagy. Dev Cell 2009; 17:98-109.

23. Okamoto K, Kondo-Okamoto N, Ohsumi Y. Mitochondria-anchored receptor Atg32 mediates degradation of mitochondria via selective autophagy. Dev Cell 2009; 17:87-97.

24. Orvedahl A, Sumpter R, Jr., Xiao G, Ng A, Zou Z, Tang Y, Narimatsu M, Gilpin C, Sun Q, Roth M, et al. Image-based genome-wide siRNA screen identifies selective autophagy factors. Nature 2011; 480:113-7.

25. Cai Q, Zakaria HM, Simone A, Sheng ZH. Spatial parkin translocation and degradation of damaged mitochondria via mitophagy in live cortical neurons. Curr Biol 2012; 22:545-52.

26. Geisler S, Holmstrom KM, Skujat D, Fiesel FC, Rothfuss OC, Kahle PJ, Springer W. PINK1/Parkin-mediated mitophagy is dependent on VDAC1 and p62/SQSTM1. Nat Cell Biol 2010; 12:119-31.

27. Kim NC, Tresse E, Kolaitis RM, Molliex A, Thomas RE, Alami NH, Wang B, Joshi A, Smith RB, Ritson GP, et al. VCP is essential for mitochondrial quality control by PINK1/Parkin and this function is impaired by VCP mutations. Neuron 2013; 78:65-80.

28. Son JH, Chun HS, Joh TH, Cho S, Conti B, Lee JW. Neuroprotection and neuronal differentiation studies using substantia nigra dopaminergic cells derived from transgenic mouse embryos. J Neurosci 1999; 19:10-20.

29. Narendra DP, Jin SM, Tanaka A, Suen DF, Gautier CA, Shen J, Cookson MR, Youle RJ. PINK1 is selectively stabilized on impaired mitochondria to activate Parkin. PLoS Biol 2010; 8:e1000298.

30. Lazarou M, Jin SM, Kane LA, Youle RJ. Role of PINK1 binding to the

TOM complex and alternate intracellular membranes in recruitment and activation of the E3 ligase Parkin. Dev Cell 2012; 22:320-33.

31. Lever M, Slow S. The clinical significance of betaine, an osmolyte with a key role in methyl group metabolism. Clin Biochem 2010; 43:732-44.

32. Lin CS, Wu RD. Choline Oxidation and Choline Dehydrogenase. J Protein Chem 1986; 5:193-200.

33. Huang S, Lin Q. Functional expression and processing of rat choline dehydrogenase precursor. Biochem Biophys Res Commun 2003; 309:344-50.

34. Reichert AS, Neupert W. Contact sites between the outer and inner membrane of mitochondria-role in protein transport. Biochim Biophys Acta 2002; 1592:41-9.

35. Chu CT, Ji J, Dagda RK, Jiang JF, Tyurina YY, Kapralov AA, Tyurin VA, Yanamala N, Shrivastava IH, Mohammadyani D, et al. Cardiolipin externalization to the outer mitochondrial membrane acts as an elimination signal for mitophagy in neuronal cells. Nat Cell Biol 2013; 15:1197-205.

36. Pankiv S, Clausen TH, Lamark T, Brech A, Bruun JA, Outzen H, Overvatn A, Bjorkoy G, Johansen T. p62/SQSTM1 binds directly to Atg8/LC3 to facilitate degradation of ubiquitinated protein aggregates by autophagy. J Biol Chem 2007; 282:24131-45.

37. Jin SM, Youle RJ. PINK1- and Parkin-mediated mitophagy at a glance. J Cell Sci 2012; 125:795-9.

38. Watanabe Y, Tanaka M. p62/SQSTM1 in autophagic clearance of a non-

ubiquitylated substrate. J Cell Sci 2011; 124:2692-701.

39. Gal J, Strom AL, Kwinter DM, Kilty R, Zhang J, Shi P, Fu W, Wooten MW, Zhu H. Sequestosome 1/p62 links familial ALS mutant SOD1 to LC3 via an ubiquitin-independent mechanism. J Neurochem 2009; 111:1062-73.

40. Exner N, Lutz AK, Haass C, Winklhofer KF. Mitochondrial dysfunction in Parkinson's disease: molecular mechanisms and pathophysiological consequences. EMBO J 2012; 31:3038-62.

41. Mandemakers W, Morais VA, De Strooper B. A cell biological perspective on mitochondrial dysfunction in Parkinson disease and other neurodegenerative diseases. J Cell Sci 2007; 120:1707-16.

42. Deas E, Plun-Favreau H, Gandhi S, Desmond H, Kjaer S, Loh SH, Renton

AE, Harvey RJ, Whitworth AJ, Martins LM, et al. PINK1 cleavage at position A103 by the mitochondrial protease PARL. Hum Mol Genet 2011; 20:867-79.

43. Lee JY, Nagano Y, Taylor JP, Lim KL, Yao TP. Disease-causing mutations in parkin impair mitochondrial ubiquitination, aggregation, and HDAC6-dependent mitophagy. J Cell Biol 2010; 189:671-9.

44. Narendra D, Kane LA, Hauser DN, Fearnley IM, Youle RJ. p62/SQSTM1 is required for Parkin-induced mitochondrial clustering but not mitophagy; VDAC1 is dispensable for both. Autophagy 2010; 6:1090-106.

45. Wilson MI, Gill DJ, Perisic O, Quinn MT, Williams RL. PB1 domain-mediated heterodimerization in NADPH oxidase and signaling complexes of atypical protein kinase C with Par6 and p62. Mol Cell 2003; 12:39-50.

46. Lamark T, Perander M, Outzen H, Kristiansen K, Overvatn A, Michaelsen E, Bjorkoy G, Johansen T. Interaction codes within the family of mammalian Phox and Bem1p domain-containing proteins. J Biol Chem 2003; 278:34568-81.

47. Okatsu K, Saisho K, Shimanuki M, Nakada K, Shitara H, Sou YS, Kimura M, Sato S, Hattori N, Komatsu M, et al. p62/SQSTM1 cooperates with Parkin for perinuclear clustering of depolarized mitochondria. Genes Cells 2010; 15:887-900.

48. Lee JY, Koga H, Kawaguchi Y, Tang W, Wong E, Gao YS, Pandey UB, Kaushik S, Tresse E, Lu J, et al. HDAC6 controls autophagosome maturation essential for ubiquitin-selective quality-control autophagy. EMBO J 2010; 29:969-80.

49. Liu L, Feng D, Chen G, Chen M, Zheng Q, Song P, Ma Q, Zhu C, Wang R, Qi W, et al. Mitochondrial outer-membrane protein FUNDC1 mediates hypoxia-induced mitophagy in mammalian cells. Nat Cell Biol 2012; 14:177-85.

50. Novak I, Dikic I. Autophagy receptors in developmental clearance of mitochondria. Autophagy 2011; 7:301-3.

51. Pyo JO, Yoo SM, Ahn HH, Nah J, Hong SH, Kam TI, Jung S, Jung YK. Overexpression of Atg5 in mice activates autophagy and extends lifespan. Nat Commun 2013; 4:2300.

52. Park S, Lee KM, Ju JH, Kim J, Noh DY, Lee T, Shin I. Protein expression profiling of primary mammary epithelial cells derived from MMTV-neu mice revealed that HER2/NEU-driven changes in protein expression are functionally clustered. IUBMB Life 2010; 62:41-50.

# 국문 초록

## 새로운 Mitophagy 조질인자로서의 CHDH 기능 연구

CHDH (choline dehydrogenase) 는 choline을 betaine aldehyde로 전환시키는 효소이고 미토콘드리아에 존재한다. 본 연구에서는 이미 알려져 있는 효소의 기능과는 별개로, mitophagy에서 CHDH의 역할을 밝혔다. CHDH의 발현을 저해시키면 CCCP에 의해 유도되는 mitophagy가 정상적으로 일어나지 않아 탈분극된 미토콘드리아의 제거가 저해되었으며, CHDH를 과발현 시켰을 때에는 mitophagy가 좀 더 활발히 일어났다. 이러한 현상은 이미 mitophagy에 중요하다고 잘 알려져 있는 PARK2와 연계되어 일어났다. CHDH는 종래 보고와는 달리 미토콘드리아의 내막과 외막에 동시에 존재했으며 mitophagy가 유도될 때 외막의 CHDH가 좀 더 증가함을 관찰하였다. PARK2의 E3 ligase 기능에 의한 기질들의 ubiquitination에 의해 mitophagy가 일어난다는 기존 보고와 달리, CHDH는 PARK2의 기질이 아니었다. PARK2와 무관하게

SQSTM1과 결합함으로써 mitophagy를 매개했고, CHDH의 FB1 도메인이 SQSTM1과의 결합에 중요함을 밝혔다. 따라서, FB1 도메인만 세포질에 과발현 시키면 SQSTM1과 경쟁적으로 결합함으로써 mitophagy를 저해함을 관찰할 수 있었다. CHDH는 SQSTM1과 결합한 뒤, LC3와 3중 구조를 형성함으로써 autophagosome을 미토콘드리아쪽으로 유도할 수 있었으며, CCCP에 의한 mitophagy 뿐만 아니라, MPP+에 의해 유도되는 mitophagy에도 CHDH가 기능하고 있었다. 결론적으로, CHDH는 mitophagy의 cargo 인식단계에서 SQSTM1과 결합함으로써 PARK2에 의한 mitophagy에 중요한 역할을 담당함을 알 수 있다.

# Part Ⅱ

## Essential role of pyruvate in PINK1 stabilization for mitophagy

# ABSTRACT

Damaged mitochondria are targeted for degradation by an autophagy pathway known as mitophagy. Despite efforts to unravel the mechanisms underlying mitophagy, aspects of mitophagy regulation remain largely unknown. In this study, by using a cell-based fluorescence assay reflecting CCCP-induced mitophagy to screen a mitochondrial protein cDNA library, we identified PDK4 as a mitophagy regulator. PDK4 enhanced pyruvate levels in both cytosol and mitochondria, and the pyruvate was required to stabilize PINK1 during mitochondrial depolarization. Accordingly, mitochondrial degradation was not efficient in the absence of pyruvate. This pyruvate-mediated mitophagy was not affected by OXPHOS or cellular ATP level, thus independent of energy metabolism. Rather, pyruvate was required for the interaction between PINK1 and TOMM20 under CCCP condition and thus for subsequent PARK2 translocation and LC3 recruitment onto depolarized mitochondria. My results suggest that pyruvate is required for CCCP-induced PINK1/PARK2-mediated

mitophagy.

*Key word*: Mitophagy, PDK4, pyruvate, PINK1, Parkinson's disease

Student Number : 2009-30857

# TABLE OF CONTENTS

# LIST OF FIGURES

# 1. INTRODUCTION

Depolarized or impaired mitochondria are cleared by autophagic machinery during a process known as mitophagy. Mitophagy is part of a mitochondrial quality control system that coordinates mitochondrial dynamics, biogenesis, fission, and fusion; mitophagy dysfunction is thus associated with human diseases.[1] Two recessive Parkinson's disease (PD) genes, PINK1/PARK6 and PARK2/parkin, are key regulators of mitophagy. Although cell type and condition-specific factors for mitophagy were not clearly determined yet, there has been a great advance to understand the machinery and underlying mechanisms involved in mitophagy during recent years.[2-4] Under carbonyl cyanide *m*-chlorophenyl hydrazone (CCCP) condition, accumulation of PINK1 on the mitochondrial outer membrane (OM) and the subsequent translocation of PARK2 to damaged mitochondria induce mitophagy.[5] However, identification of regulatory molecules in this process remains to be elucidated. Newly found novel mitophagy regulators are basically involved in

autophagic machinery[1] or reside on mitochondrial OM.[6] Or, they could be lipid[7] and metal.[8] However, metabolic approaches to mitophagy were not noticeable.

Pyruvate is produced by the glycolysis pathway and serves as an important intermediary metabolite for the maintenance of cellular homeostasis by acting as a "fuel" for mitochondrial respiration.[9, 10] Although it has been long period of our knowledge for pyruvate, specific carrier for pyruvate across the mitochondrial membrane was recently identified, termed mitochondrial pyruvate carrier (MPC).[11, 12] The metabolic reaction of mitochondrial pyruvate is regulated by the pyruvate dehydrogenase complex (PDC), which catalyzes the oxidation of pyruvate to acetyl CoA in the mitochondrial matrix and is responsible for many age-associated diseases.[13, 14] In addition to its well-known role in the bioenergetics of the mitochondrial citric acid cycle, the protective effect of pyruvate on ischemic damage has been extensively studied over the last two decades.[15-18] Interestingly, pyruvate's role in ischemic damage is attributed to its anti-oxidative function,[19, 20] which also contributes to its role in cancer progression under hypoxic conditions[21] and to its

ability to mitigate myocardial infarction.[22, 23] PDC activity is governed by pyruvate dehydrogenase kinase (PDK) which is regulated by the cellular level of pyruvate, acetyl Co-A, NADH and ATP.[24] There is four isoform, PDK1, 2, 3, and 4 which are expressed tissue-specifically and differently modulates PDC activity.[25-28]

Among these isoforms, PDK4 is highly expressed in skeletal muscle, heart and liver[29, 30] that require high level of oxidation. And PDK4 negatively regulates PDC activity in response to changing nutrient levels.[29, 31, 32] In agreement with this function, loss of PDK4 in *pdk4*$^{-/-}$ mice lowers glucose level and ameliorates glucose tolerance in diet-induced obese mice.[33] The expression level of PDK4 is affected by various factors[24], including starvation.[34] Regarding autophagy, PDK4 leads to AMPK activation and subsequent mTOR inhibition.[35] Recently, a genome-wide siRNA screening study reported that knockdown of PDK4 expression affects CCCP-induced mitophagy.[3] Although these reports implicate that PDK4 regulates autophagy/mitophagy, it needs to be solved how PDK4 regulates autophagy/mitophagy.

To identify the novel modulator of mitophagy, I performed a functional screening by using a cDNA expression library encoding mitochondrial proteins. Interestingly, PDK4 was isolated as the most effective clone which enhanced CCCP-induced mitochondria degradation. PDK4 affected mitophagy through upregulation of pyruvate level and PINK1 stabilization.

# 2. MATERIALS AND METHODS

## 2.1. Functional screening of mitophagy regulators

HEK293T cells grown on multi-well culture plates were co-transfected with Mito-GFP and cDNA expression vectors for 24 h and then treated with 100 μM CCCP for 2 h. The intensities of GFP signals were measured using the ENVISION Multilabel Plate Reader (Perkin Elmer). The cDNA clones showing more than 10% reduction in GFP intensity compared to that in the control were first selected. The positive clones were further analyzed for their effects on mitophagy by western blotting using mitochondrial marker proteins.

## 2.2. Cell lines and culture

Cells were grown in DMEM (HyClone, SH30243.01) supplemented with 10% fetal bovine serum (FBS) (HyClone, SH30919.03) and 50 U/mL each of penicillin and streptomycin, and were incubated at 37°C in an atmosphere containing 5% $CO_2$.

For experiments testing the effects of pyruvate, pyruvate-negative DMEM (SH30022) containing the same concentrations of FBS, penicillin and streptomycin was used. For glutamine-induced mitophagy, Leibovitz L-15 Medium (HyClone, SH30525) was modified to contain 25 mM glucose with basal 2 mM glutamine (Glucose group) or no glucose with 4 mM glutamine (Glutamine group).

### 2.3. Plasmids and transfection

PDK4-HA was produced by subcloning PDK4 into pcDNA3-HA (Invitrogen). PARK2-GFP, GFP-GABARAPL1, GFP-GABARAPL2, and GFP-BNIP3L were constructed by subcloning target sequences into pEGFP vector (Invitrogen). Flag-PARK2 and mRFP-LC3 were subcloned into p3XFLAG-CMV (Sigma Aldrich) and pDsRed-Monomer (BD Bioscience) vectors, respectively. GFP-LC3 has been described previously[36] and PINK1-GFP was kindly gifted by Dr. J. Chung (Seoul National University, Korea). DNA transfections were performed with PolyFect reagent (Qiagen, 1015586) for 24 h, according to the manufacturer's instructions.

## 2.4. Immunofluorescence microscopy and determination of colocalization coefficient

Cells grown on a coverslip were fixed with 4% paraformaldehyde and permeabilized with 0.01% digitonin. After blocking with 10% fetal bovine serum, cells were incubated with primary antibodies at dilutions ranging from 1:100 to 1:250, and subsequently with an Alexa Fluor-conjugated secondary antibody (Molecular Probes). Samples were visualized with a confocal laser scanning microscope (Carl Zeiss, LSM700). ZEN software (Carl Zeiss) and the images were subjected to the analysis of the colocalization coefficient.

## 2.5. Measurement of pyruvate and ATP

Pyruvate and ATP levels were determined by using the Pyruvate Colorimetric/Fluorometric Assay Kit (BioVision, K609-100) and the ENLITEN ATP Assay System Bioluminescence Detection Kit (Promega, FF2000), respectively.

## 2.6. Immunoprecipitation, western blot, and antibodies

Immunoprecipitation and western blot assays were performed as described previously[37]. After samples were separated by SDS-PAGE and transferred onto nitrocellulose membrane (Pall Corporation, 66485), the membranes were blocked with 5% skim milk and incubated with the following antibodies: HA (Santa Cruz, sc-805), ACTB (sc-47778), TOMM20 (sc-17764), CANX (sc-11397), GFP (sc-8334), TUBA (sc-23948), CHDH (sc-102442), LC3 (Novus Biologicals, NB100-2220), TIMM23 (BD Bioscience, 611222), SOD2 (Upstate, 06-984), COX4I1 (Abcam, ab14744-100), PINK1 (Novus Biologicals, BC100-494; Santa Cruz, sc-33796) and FLAG (Sigma Aldrich, F3165). The blots were detected using the enhanced chemiluminescence (ECL) method.

## 2.7. Transmission electron microscopy

Cells were fixed with 3% paraformaldehyde and 0.5% glutaraldehyde in

phosphate-buffered saline (PBS) at 4°C for 2 h. After serial dehydration with 70%, 95%, and 100% ethanol for 30 min twice, London Resin White (Polyscience, 17411-500) was used for infiltration for 24 h. During that time, the resin was refreshed at 8-h intervals. Polymerization was performed overnight at 50°C. Sectioned specimens were placed on the Formvar-coated nickel grid (Polyscience, 300 meshes, 24928) and stained with 2% uranyl acetate and Reynold's lead citrate for 7 min each. Samples were washed with distilled water and then visualized under a transmission electron microscope (JEOL, JEM1010) at 80 kV.

## 2.8. Mitochondrial fractionation

Mitochondrial fractionation by differential centrifugation was performed as described previously[37].

## 2.9. Measurement of mitochondrial membrane potential by

### Tetramethylrhodamine, ethyl ester (TMRE)

Cells were stained with 100 nM TMRE for 20 min, rinsed with PBS to remove excess dye, and then replaced in their original growth medium. The signal intensity of TMRE was captured by a fluorescence microscope and analyzed using the ImageJ program.

## 2.10. Statistical analysis

Quantitative data are represented as mean ± standard deviation. Statistical significance was determined using Student's *t*-test and *P*-value < 0.05 was deemed statistically significant.

# 3. RESULTS

## 3.1. Functional screening of mitochondrial proteins identified PDK4 as a mitophagy stimulator

To discover the novel factor(s) that regulate mitophagy, I established a cell-based assay and performed a gain-of-function screening by using 437 cDNAs encoding mitochondrial proteins, as described in Methods (**Fig. 1A**). HEK293T cells were co-transfected with an individual cDNA and Mito-GFP, a mito-tracker,[37] and then exposed to a high dose of CCCP (100 μM) for a short time to induce acute depolarization and rapid degradation of the mitochondria. I isolated five putative positive clones, which reduced the fluorescence of Mito-GFP relative to the levels of fluorescence in control cells (**Fig. 1B**). Among them, PDK4 appeared to have the strongest effect on the fluorescence of Mito-GFP.

To further characterize the effects of PDK4 overexpression on mitophagy, I examined LC3-II conversion in PDK4-expressing cells. Ectopic expression of PDK4

in HEK293T cells increased LC3-II conversion *per se* after treatment with 10 M CCCP, while no difference was observed in untreated cells (**Fig. 1C**). LC3-II conversion was further enhanced in the presence of the vacuolar-type $H^+$-ATPase inhibitor bafilomycin $A_1$. When I incubated HeLa cells with CCCP and performed immunocytochemical analysis of mitochondria by using the mitochondrial TOMM20 antibody, PDK4 overexpression greatly accelerated PARK2-mediated mitochondrial clearance (**Fig. 2A**). Western blot analysis similarly indicated accelerated degradation of the mitochondrial proteins TIMM23 and TOMM20 owing to PDK4 overexpression, while endoplasmic reticulum-bound protein CANX/calnexin and the cytosolic protein TUBA/tubulin were unaffected (**Fig. 2B, C**). Together, these results suggest that PDK4 functions to regulate CCCP-induced mitophagy.

### 3.2. Increased pyruvate levels owing to PDK4 overexpression enhance mitophagy

Because PDK4 is one of the pyruvate dehydrogenase kinases known to inhibit PDC activity, I thought it unlikely that PDK4-regulated pyruvate levels would

affect mitophagy. I found that PDK4 overexpression increased pyruvate levels by 40% in both the mitochondrial and the cytosolic fractions of HEK293T cells (**Fig. 3A**), as previously reported.[38] Because cDNA screening indicated that both PDK3 and PKD4 could affect mitophagy in the transfected cells, (**Fig. 1B**), I more closely examined the effects of PDK family members on pyruvate levels. Among the members of the PDK family, overexpression of PDK4 had a significant effect on pyruvate levels in both mitochondrial and cytosolic fractions, while PDK3 had a modest, but insignificant effect (**Fig. 3B**). In contrast, PDK1 and PDK2 did not affect pyruvate levels. Interestingly, the cellular levels of pyruvate owing to PDK4 overexpression were similar to the levels resulting from pyruvate treatment of untransfected cells (**Fig. 3B**, +Pyr), and these levels did not increase further when PKD4-overexpressing cells were treated with pyruvate (**Fig. 3B**, PDK4+Pyr). These results indicated that PDK4 might function through pyruvate to regulate mitophagy in HEK293T cells.

To test this hypothesis, I used western blotting to monitor mitophagy in the absence or presence of pyruvate (**Fig. 3C**). The mitochondrial proteins TOMM20,

TIMM23, SOD2, COX4I1, and CHDH, but not the cellular proteins CANX and TUBA, were degraded by CCCP treatment, and their degradation was augmented by pyruvate treatment. Similar results were observed with confocal image analysis showing that the clearance of Mito-RFP was enhanced from 15.2% to 38.2% by pyruvate treatment (**Fig. 3D**). Furthermore, electron microcopy revealed extensive digestion of mitochondria in the autophagic vesicles in the presence of pyruvate, while in the absence of pyruvate, the inner membrane (IM) structure of mitochondria and fragmented mitochondria still remained in the vesicles (**Fig. 4A, B**). Collectively, these results suggest that pyruvate stimulates mitophagy via a mechanism that is dependent on the ability of PDK4 to increase pyruvate levels.

### 3.3. Pyruvate-mediated mitophagy is independent of energy metabolism

Since pyruvate is the major energy source for aerobic respiration and is related to cellular energetics, I considered the mechanism linking energy metabolism to mitophagy. I first wondered whether PDK4 overexpression and pyruvate treatment

might regulate ATP production. Measurement of ATP levels revealed that PDK4 overexpression lowered ATP content in both the cytosol and the mitochondria, while pyruvate treatment increased it (**Fig. 5A**). Because PDK4 and pyruvate both stimulate mitophagy, these results suggest that neither PDK4-mediated nor pyruvate-mediated mitophagy is associated with ATP content. Recently, Melser *et al* reported that glutamine-induced oxidative phosphorylation activates mitophagy with a concomitant increase in ATP content.[39] Thus, I examined the association of oxidative phosphorylation with PDK4-mediated mitophagy. As previously reported, cells grown on glutamine show more degradation of mitochondrial proteins than do cells grown on glucose (**Fig. 5B**); however, overexpression of PDK4 did not affect mitochondrial protein degradation. I used the TCA cycle intermediate citrate to assess the relationship between ATP and mitophagy further (**Fig. 5C, D**). Different ATP contents by PDK4 overexpression and citrate treatment (**Fig. 5C**) were applied to the mitophagy assay using western blot (**Fig. 5D**). Supplementary citrate did not affect mitophagy compared to that observed in citrate-lacking controls, and that PDK4

expression accelerated mitochondria clearance (**Fig. 5D**). These results indicate that PDK4–pyruvate axis functions independently of OXPHOS-ATP-mediated mitophagy.

### 3.4. Pyruvate is required for PINK stabilization and enhances PARK2 and LC3 recruitment onto depolarized mitochondria

To examine the mechanism by which pyruvate stimulates mitophagy, I tested the hypothesis that pyruvate affects the interaction between mitochondrial BNIP3L/NIX and autophagosomal LC3. BNIP3L/NIX has previously been reported to mediate CCCP-induced mitophagy via its interaction with LC3.[40, 41] Using confocal microscopy, I found that pyruvate did not significantly affect the co-localization of GFP-BNIP3L/NIX and mRFP-LC3 (**Fig. 6**). Since CCCP-induced mitophagy is mediated by the accumulation of PINK1 on the OM of mitochondria and the subsequent recruitment of PARK2, I examined the effects of pyruvate on this machinery in HeLa cells. Surprisingly, I observed that CCCP induced the accumulation of PINK1 in the presence, but not in the absence, of pyruvate (**Fig. 7A**),

indicating that pyruvate is required for the stabilization of PINK. This effect of pyruvate on PINK stabilization was also observed by confocal microscopy using Mito-RFP and PINK1-GFP (**Fig. 7B**).

The current model of PINK1 processing states that PINK is cleaved by mitochondrial proteases such as PARL on the inner membrane (IM) of mitochondria and then degraded by proteasomes.[42, 43] To address what happened to PINK1 in the absence of pyruvate under CCCP treatment, I performed western blot analysis after treatment with MG132, a proteasome inhibitor (**Fig. 7C**). The result showed that in CCCP-treated cells, in the absence of pyruvate, PINK1 was cleaved and degraded rather than being accumulated on the mitochondrial OM. The cleavage and degradation were inhibited by MG132, resulting in the accumulation of the 52-kDa PINK1 fragment in the mitochondria. In contrast, in the presence of pyruvate, PINK1 was accumulated on the mitochondrial OM, as indicated by the detection of the full-length 64-kDa protein. This result further supports the necessity of pyruvate for PINK1 stabilization. Since PINK1 binds to TOMM complex during stabilization on

the mitochondrial OM under CCCP condition,[44] I addressed whether pyruvate was required for their interaction. An immuoprecipitaion analysis with endogenous TOMM20 was performed and resulted in interaction with PINK1 only in the presence of pyruvate (**Fig. 7D**). I found that this requirement for pyruvate was highly specific as the three pyruvate analogs bromopyruvate, phenylpyruvate, and α-ketobutyrate[45] were unable to stabilize PINK1 (**Fig. 7E**). Additionally, I found that pyruvate did not significantly affect mitochondrial membrane potential (MMP, **Fig. 7F**).

Next, I examined the translocation of PARK2 to depolarized mitochondria following PINK1 stabilization. Using mitochondria from HeLa cells overexpressing FLAG-PARK2, I found that CCCP-induced PARK2 recruitment onto the mitochondria increased by 4.6 fold when cells were treated with pyruvate (**Fig. 8A**). Furthermore, GFP-LC3 recruitment onto the mitochondria was also significantly increased by pyruvate, as determined by the co-localization coefficient calculated using confocal microscopy (**Fig. 8B**), suggesting that pyruvate is required for the conventional PINK1/PARK2 pathway of mitophagy. I further tested the effects of

pyruvate on the co-localization of LC3 and gamma-aminobutyric acid receptor-associated protein (GABARAP) to the mitochondria since the GABARAP was previously reported to play a role in mitophagy like LC3.[30] However, pyruvate did not affect the co-localization of LC3 and GABARAP (**Fig. 8C**). Moreover, I found that pyruvate did not affect the mitophagy mediated by choline dehydrogenase (CHDH), an important molecule for mitophagy.[27] (**Fig. 8D**)

**Figure 1. Isolation of PDK4 as a mitophagy enhancer by functional screening**

(**A**) Schematic diagram depicting the functional screening. A detailed description of the screening is provided in the Methods section.

(**B**) Genes showing high impact on the fluorescence of Mito-GFP are represented.

(**C**) Western blot analysis of cell lysates prepared from mock (DMSO)-treated or CCCP-treated HEK293T cells overexpressing PDK4-HA, either in the presence or in the absence of bafilomycin $A_1$ (Baf). The β-Actin (ACTB) served as a lane-loading control.

Figure 1

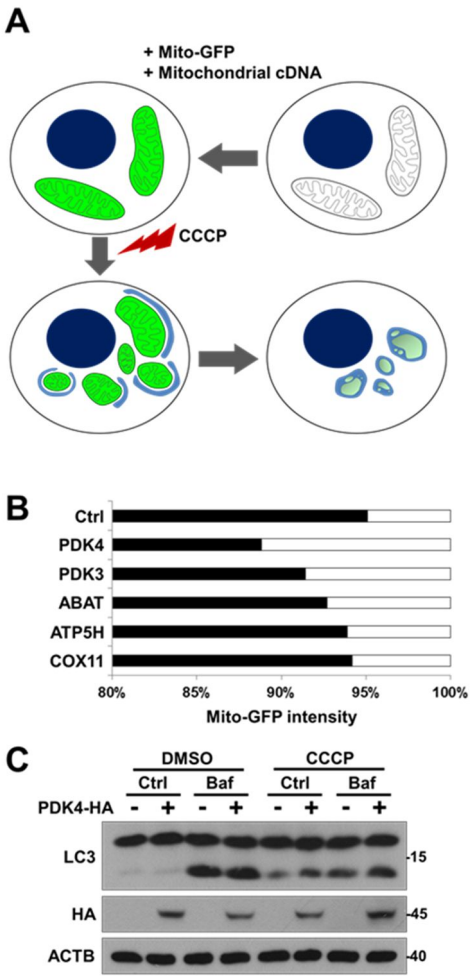
A
+ Mito-GFP
+ Mitochondrial cDNA
CCCP
B
Ctrl
PDK4
PDK3
ABAT
ATP5H
COX11
80%
85%
90%
95%
100%
Mito-GFP intensity
C
DMSO
CCCP
Ctrl
Baf
Ctrl
Baf
PDK4-HA
- + - + - + - +
LC3
HA
ACTB
-15
-45
-40

**Figure 2. Overexpression of PDK4 enhances mitophagy**

(**A**) HeLa cells were transfected with PARK2-GFP and either control vector (Ctrl) or PDK4. After treatment with 20 μM CCCP for 6 h, cells were fixed and immunostained with TOMM20 antibody. TOMM20-negative and PARK2-GFP-positive cells ($n > 100$) were counted and depicted. * $P < 0.001$.

(**B, C**) HeLa cells were transfected with PARK2-GFP and PDK4-HA, and then treated with 10 μM CCCP for 30 h. Cell lysates were analyzed with western blotting (**B**) and the signals on the blot were quantified (**C**). The α-tubulin (TUBA) served as a loading control.

Figure 2

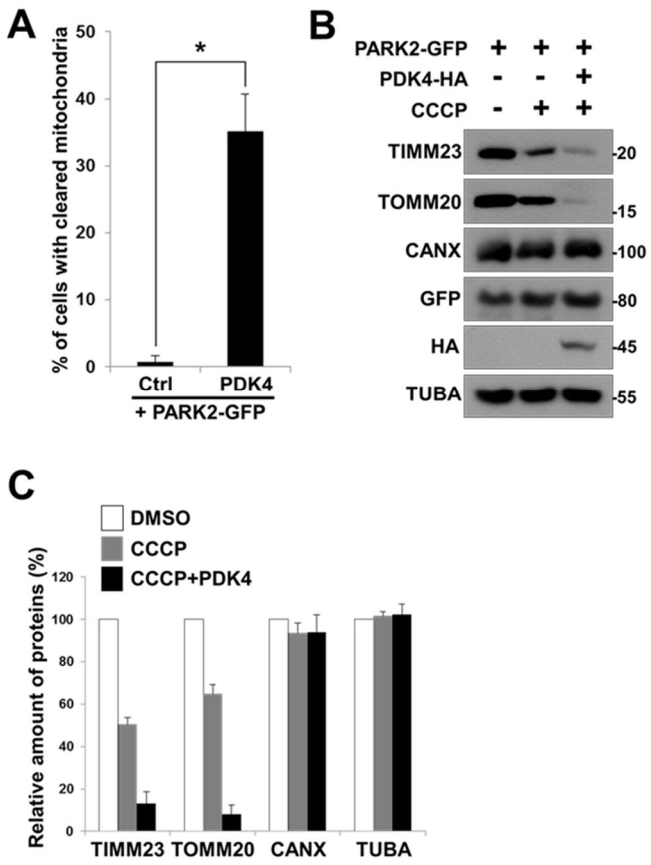
A
% of cells with cleared mitochondria
50
40
30
20
10
0
*
Ctrl
PDK4
+ PARK2-GFP
B
PARK2-GFP + + +
PDK4-HA - - +
CCCP - + +
TIMM23
TOMM20
CANX
GFP
HA
TUBA
-20
-15
-100
-80
-45
-55
C
DMSO
CCCP
CCCP+PDK4
Relative amount of proteins (%)
120
100
80
60
40
20
0
TIMM23
TOMM20
CANX
TUBA

**Figure 3. Enhanced pyruvate levels owing to PDK4 overexpression**

(**A**) HEK293T cells were transfected with either control vector (Ctrl) or PDK4 and then treated with 1 mM pyruvate for 4.5 h. Pure mitochondrial and cytosolic fractions were obtained and pyruvate levels were measured, as described in Methods. * $P <$ 0.05.

(**B**) HEK293T cells were transfected with PDK family members and were then left untreated or incubated with 1 mM pyruvate for 4.5 h. After cell lysates were fractionated into the mitochondria and the cytosol fractions, pyruvate levels in the fractions were determined as described in Methods. * $P < 0.01$, ** $P < 0.05$.

(**C**) HepG2 cells were either left untreated or treated with 1 mM pyruvate for 2 h and then exposed to 10 μM CCCP for 24 h. Cell lysates were subjected to western blot analysis.

(**D**) HeLa-Mito-RFP stable cells were transfected with PARK2-GFP and incubated with 1 mM pyruvate for 30 min prior to the treatment with 10 μM CCCP for 24 h. Lack of RFP signal under a fluorescence microscope is indicative of cleared

mitochondria. * $P < 0.05$, Scale bar = 10 μm ($n > 50$).

Figure 3

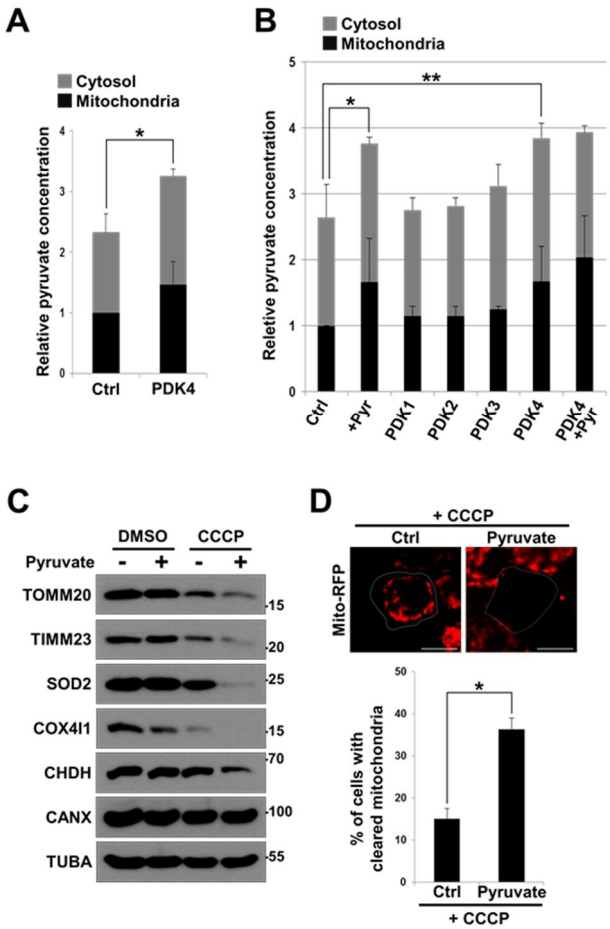
A
Cytosol
Mitochondria
Relative pyruvate concentration
Ctrl
PDK4
B
Cytosol
Mitochondria
Reletive pyruvate concentration
Ctrl
+Pyr
PDK1
PDK2
PDK3
PDK4
PDK4 +Pyr
C
DMSO
CCCP
Pyruvate
TOMM20
TIMM23
SOD2
COX4I1
CHDH
CANX
TUBA
D
+ CCCP
Ctrl
Pyruvate
Mito-RFP
% of cells with cleared mitochondria
Ctrl
Pyruvate
+ CCCP

**Figure 4. PDK4 increases mitochondrial pyruvate levels, thereby enhancing mitophagy**

(**A, B**) HepG2 cells were treated with 1 mM pyruvate for 30 min and subsequently treated with 10 μM CCCP for 2 h. Cells were observed under a transmission electron microscope. Scale bar = 1 μm (upper panel) and 200 nm (zoom-in lower panel) (**A**). The percentage of digested mitochondria in figure D was determined (**B**) ($n > 30$).

**Figure 4**

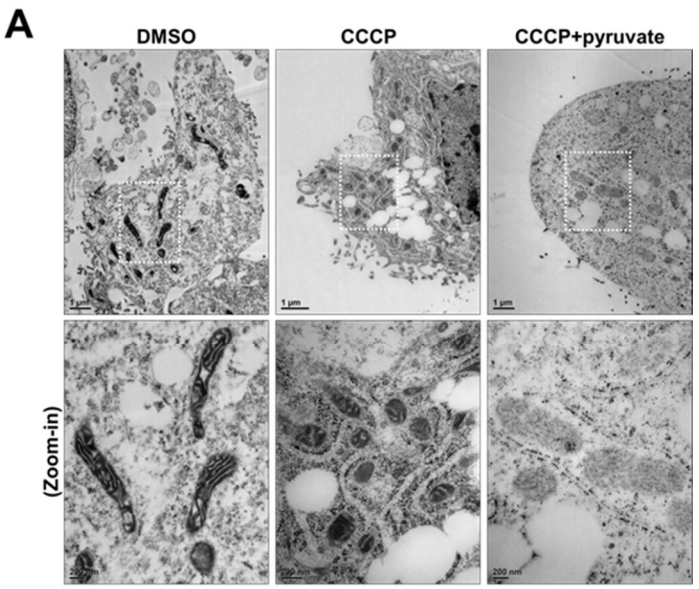
A
DMSO
CCCP
CCCP+pyruvate
(Zoom-in)
1 μm
200 nm

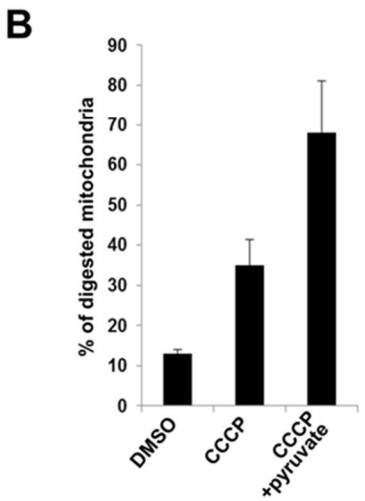
B
% of digested mitochondria
90
80
70
60
50
40
30
20
10
0
DMSO
CCCP
CCCP +pyruvate

**Figure 5. Pyruvate-mediated mitophagy is not correlated with energy metabolism**

(**A**) HEK293T cells were either transfected with PDK4 for 24 h or incubated with 1 mM pyruvate for 4.5 h. Cell extracts were prepared and separated into the cytosol and mitochondria fractions, followed by ATP assay, as described in Methods. ATP contents relative to that in the control (Ctrl) are represented.

(**B**) HeLa cells grown in either 25 mM glucose or 4 mM glutamine-containing media were transfected with PDK4-HA. After treatment with 20 μg/mL cycloheximide (CHX) for 8 h, cell extracts were prepared and analyzed by western blotting (upper). The signals on the blots were quantified (lower).

(**C**) HEK293T cells were transfected with PDK4 and then left untreated or treated with 1 mM citrate for 2 h. ATP content was measured as described in (A). * $P < 0.001$, ** $P < 0.005$.

(**D**) HEK293T cells were transfected with PDK4 and then treated with 10 μM CCCP for 24 h in the presence or absence of 1 mM citrate. Cell lysates were analyzed by

western blotting.

## Figure 5

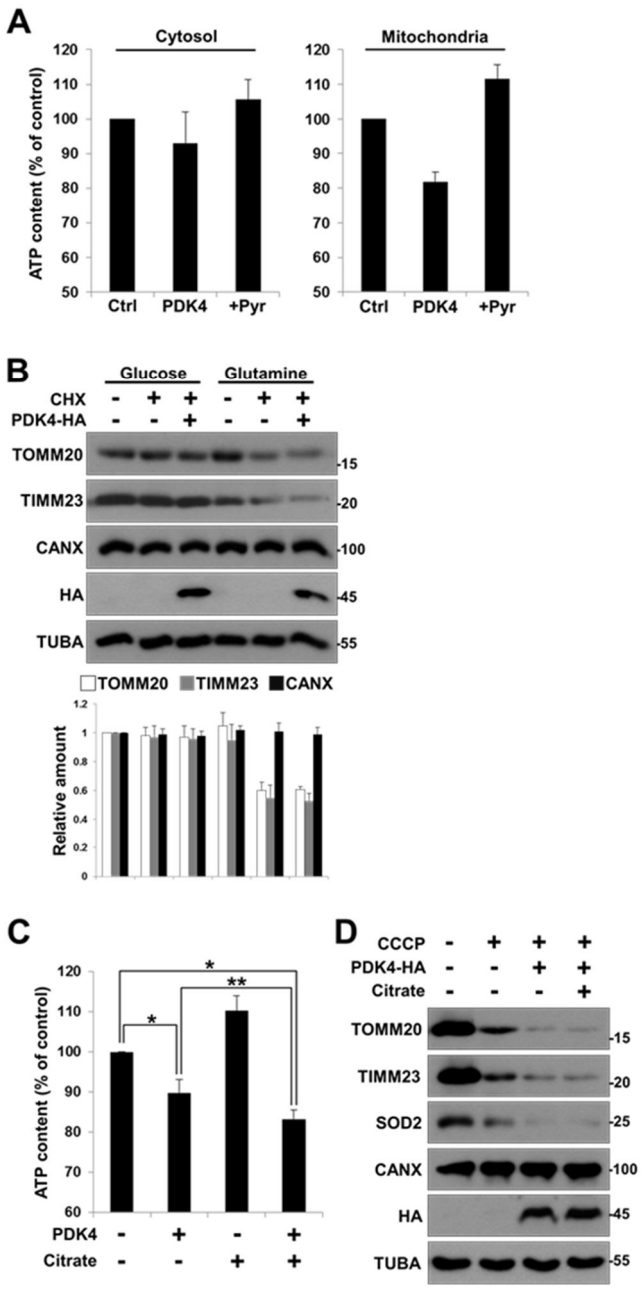
A
Cytosol
Mitochondria
ATP content (% of control)
120
110
100
90
80
70
60
50
Ctrl
PDK4
+Pyr
B
Glucose
Glutamine
CHX
PDK4-HA
TOMM20
TIMM23
CANX
HA
TUBA
15
20
100
45
55
TOMM20 TIMM23 CANX
Relative amount
1.2
1
0.8
0.6
0.4
0.2
0
C
ATP content (% of control)
*
**
PDK4
Citrate
D
CCCP
PDK4-HA
Citrate
TOMM20
TIMM23
SOD2
CANX
HA
TUBA
15
20
25
100
45
55

**Figure 6. Effect of pyruvate on BNIP3L-mediated LC3 recruitment**

HepG2 cells were cotransfected with GFP-BNIP3L and mRFP-LC3 were first treated with 1 mM pyruvate for 2 h and then with 10 μM CCCP for 30 min. Samples were analyzed by confocal microscopy. Scale bar = 10 μm (upper). Colocalization coefficients were determined from the fluorescence images (lower) ($n > 50$).

**Figure 6**

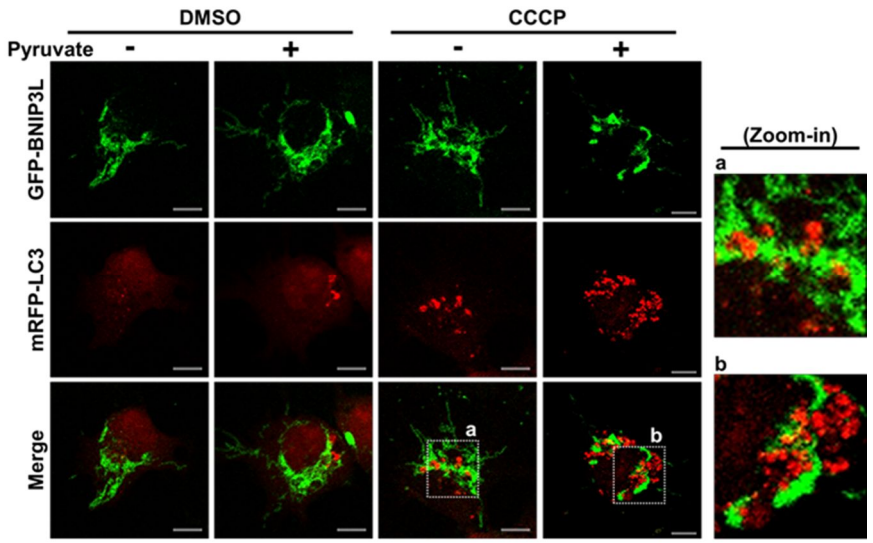
DMSO
CCCP
Pyruvate
-
+
-
+
GFP-BNIP3L
mRFP-LC3
Merge
a
b
(Zoom-in)
a
b

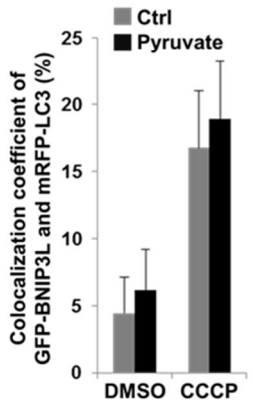
Ctrl
Pyruvate
Colocalization coefficient of GFP-BNIP3L and mRFP-LC3 (%)
25
20
15
10
5
0
DMSO
CCCP

**Figure 7. Pyruvate induces PINK1 stabilization**

(**A**) HeLa cells were either left untreated or were incubated with 1 mM pyruvate for 2 h, followed by treatment with 10 μM CCCP for 2 h. Cell extracts were analyzed by western blotting.

(**B**) PINK1-GFP and Mito-RFP were transfected into HeLa cells, and the cells were subjected to treatment with 1 mM pyruvate for 2 h before treatment with 10 μM CCCP for 3 h. Samples were fixed and analyzed by confocal microscopy. Scale bar = 10 μm.

(**C**) HeLa cells were incubated with 1 mM pyruvate or 10 μM MG132 for 2 h and then exposed to 10 μM CCCP for 3 h. Mitochondria were then purified and analyzed by western blotting.

(**D**) HeLa cells were pretreated with 1 mM pyruvate for 1 h and then treated with 10 μM CCCP for 3 h. Pure mitochondria were obtained and subjected to immunoprecipitation with TOMM20 antibody.

(**E**) HeLa cells were first treated with 1 mM pyruvate or the pyruvate analogs

bromopyruvate (BR), phenylpyruvate (PH), and α-ketobutyrate (KE) for 2 h, and then with 10 μM CCCP for 2 h. The cells were then subjected to western blotting.

(**F**) HeLa cells were treated with 1 mM pyruvate for 2 h prior to the treatment with 10 μM CCCP for 1 h. Cells were stained with TMRE solution and analyzed as described in Methods. N.S., not significant (* $P > 0.05$).

Figure 7

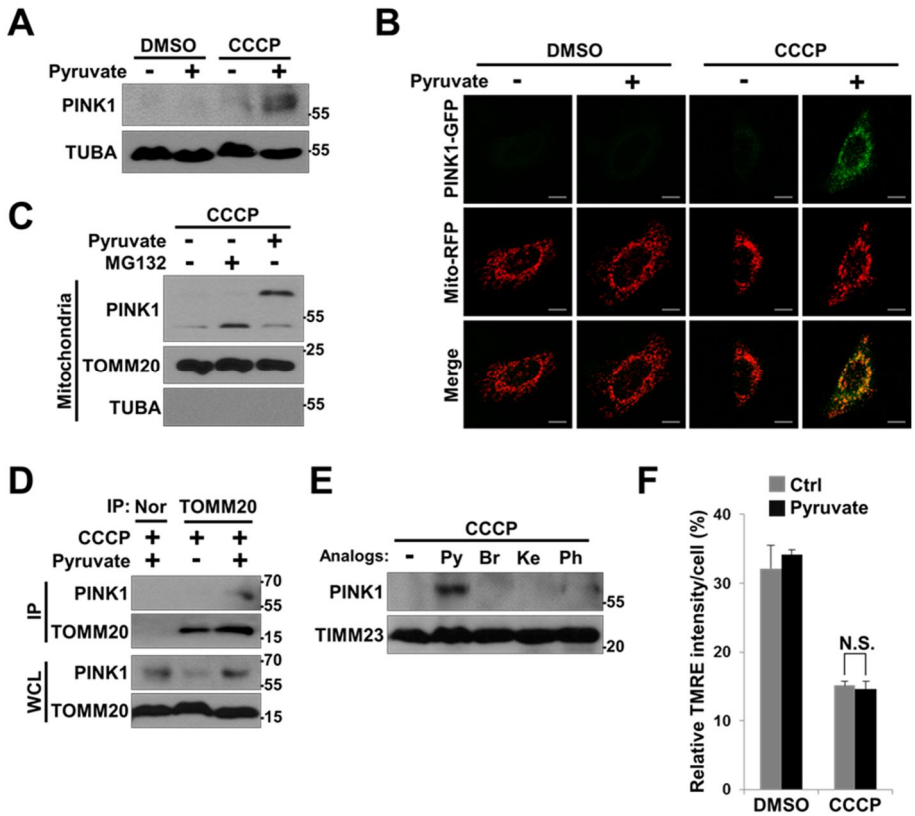
A
DMSO
CCCP
Pyruvate - + - +
PINK1
TUBA
55
55
B
DMSO
CCCP
Pyruvate - + - +
PINK1-GFP
Mito-RFP
Merge
C
CCCP
Pyruvate - - +
MG132 - + -
Mitochondria
PINK1
TOMM20
TUBA
55
25
55
D
IP: Nor TOMM20
CCCP + + +
Pyruvate + - +
IP
PINK1
TOMM20
WCL
PINK1
TOMM20
70
55
15
70
55
15
E
CCCP
Analogs: - Py Br Ke Ph
PINK1
TIMM23
55
20
F
Ctrl
Pyruvate
Relative TMRE intensity/cell (%)
40
30
20
10
0
N.S.
DMSO
CCCP

**Figure 8. Pyruvate enhances PARK2 translocation and LC3 recruitment onto depolarized mitochondria**

(**A**) HeLa cells were transfected with FLAG-PARK2 and incubated with 1 mM pyruvate for 2 h before the treatment with 10 μM CCCP for 2 h. Then, the mitochondrial fraction was prepared and analyzed by western blotting. The signal of mitochondrial FLAG-PARK2 on the blot was quantified and represented as a fold change relative to that of whole cell lysate (WCL).

(**B**) After being transfected with FLAG-PARK2, Mito-RFP, and GFP-LC3, HeLa cells were treated with 1 mM pyruvate for 2 h prior to the treatment with 10 μM CCCP for 4 h. Cells were fixed and observed under a confocal microscope (right). Colocalization coefficient was determined from the fluorescence images (left). Scale bar = 10 μm. * $P < 0.005$ ($n > 50$).

(**C**) HeLa cells were cotransfected with Mito-RFP and GFP-LC3, GFP-GABARAPL1, or GFP-GABARAPL2. After incubation with 1 mM pyruvate for 30 min, cells were treated with 10 μM CCCP for 4 h and then analyzed by confocal microscopy.

Colocalization coefficients were measured as described in Methods. * $P < 0.001$ ($n > 50$).

(**D**) HeLa and HeLa-shCHDH knockdown cells were transfected with FLAG-PARK2 and then treated with 1 mM pyruvate for 2 h before exposure to 10 μM CCCP for 24 h. After immunostaining with TOMM20 antibody, the numbers of TOMM 20-negative and GFP-positive cells were counted and represented ($n > 100$).

Figure 8

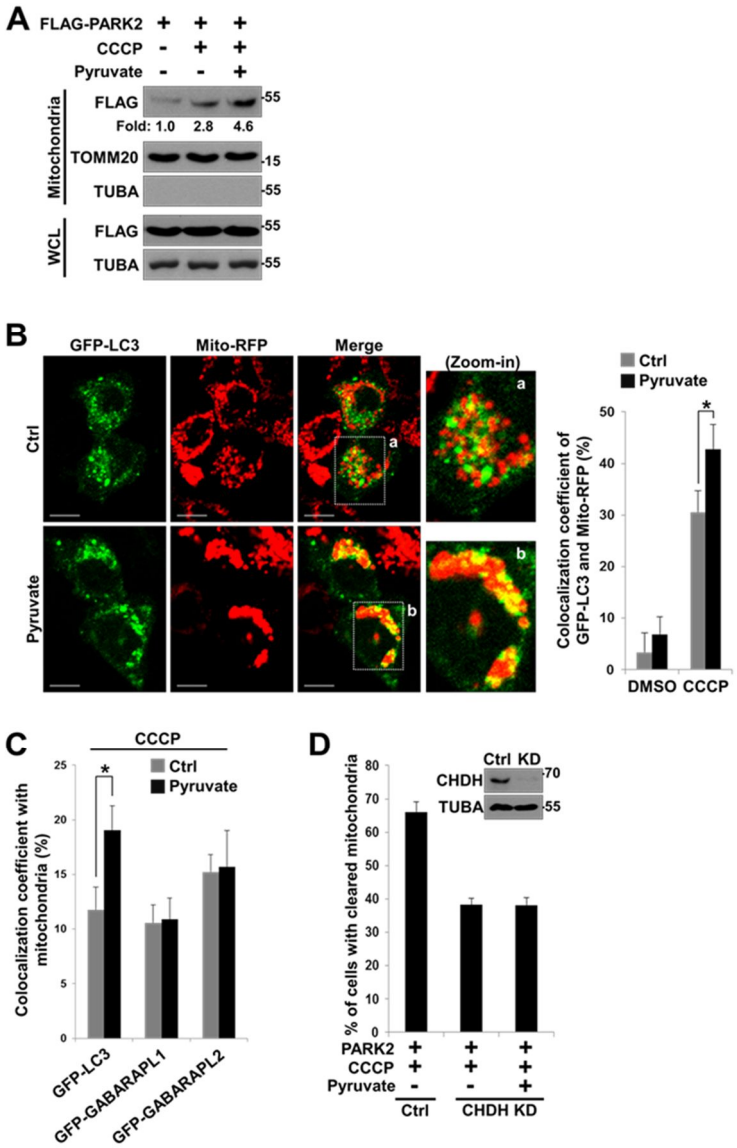
A
FLAG-PARK2 + + +
CCCP - + +
Pyruvate - - +
Mitochondria
FLAG
Fold: 1.0 2.8 4.6
TOMM20
TUBA
WCL
FLAG
TUBA
-55
-15
-55
-55
-55
B
GFP-LC3
Mito-RFP
Merge
(Zoom-in)
Ctrl
Pyruvate
a
b
Ctrl
Pyruvate
Colocalization coefficient of GFP-LC3 and Mito-RFP (%)
DMSO CCCP
C
CCCP
Ctrl
Pyruvate
Colocalization coefficient with mitochondria (%)
GFP-LC3
GFP-GABARAPL1
GFP-GABARAPL2
D
Ctrl KD
CHDH
TUBA
% of cells with cleared mitochondria
PARK2
CCCP
Pyruvate
Ctrl
CHDH KD

**Figure 9. Proposed model for mitophagy.**

Mitochondrial depolarization induces PINK1 stabilization on the OM which requires pyruvate. Once PINK1 is stabilized, PARK2-mediated ubiquitination of substrates and PARK2-independent interaction between CHDH and SQSTM1 recruits LC3-anchored autophagosome to the mitochondria, and destine to degradation.

Figure 9

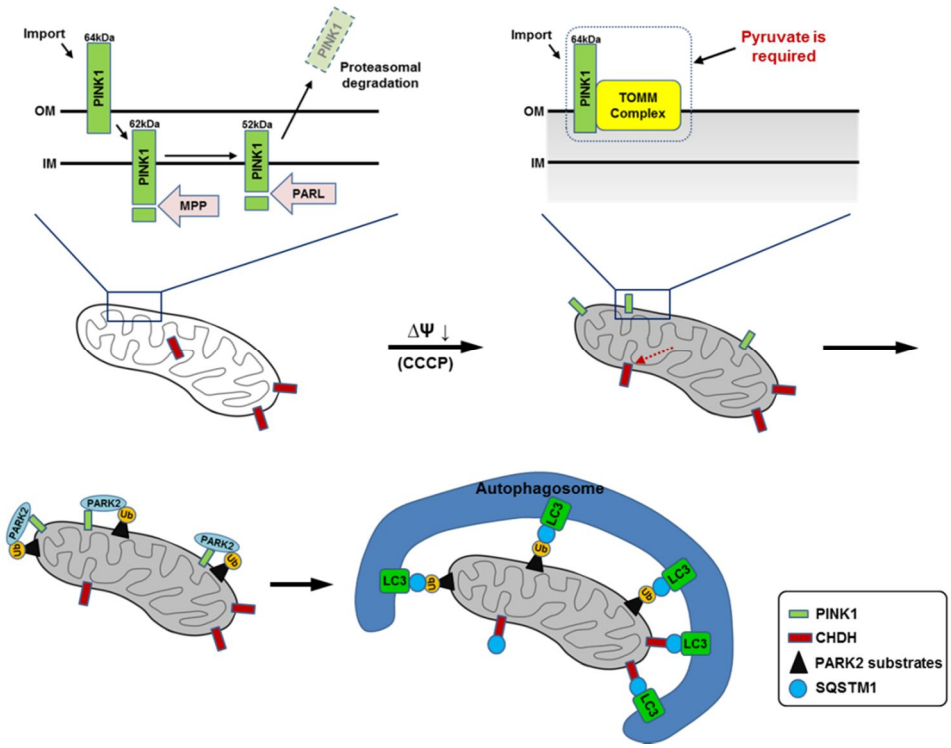
Import
64kDa
PINK1
OM
IM
62kDa
52kDa
PINK1
PINK1
Proteasomal degradation
MPP
PARL
Import
64kDa
PINK1
Pyruvate is required
TOMM Complex
OM
IM
ΔΨ ↓
(CCCP)
PARK2
Ub
Autophagosome
LC3
PINK1
CHDH
PARK2 substrates
SQSTM1

# 4. DISCUSSION

In this study, PDK4 is regarded as a potential regulator that affects autophagy or mitophagy. PDK4 is known to be upregulated under fasting condition[34] and leads to AMPK activation and mTOR inhibition[35]. In addition, a genome-wide siRNA screening study shows a possibility that PDK4 knockdown affects mitophagy in response to CCCP treatment[3]. Thus, PDK4 is supposed to regulate autophagy/mitophagy. However, there has been a remaining last piece of puzzle to elucidate the role of PDK4 in autophagy/mitophagy. Here, we provide a piece of evidence linking PDK4 to mitophagy rather than macroautophagy. LC3 conversion triggered by PDK4 was only observed in the presence of CCCP. In addition, subsequent mitophagic events, including elucidation for the role of PDK4 as a stabilizer of PINK1, collectively suggest that PDK4 functions in the mitochondria-targeted process. Further, the strongest effect of PDK4 among PDK isoforms on the

increase of pyruvate level adds more evidence that PDK4 plays a role mainly in mitophagy.

As the mechanism of PDK4 function in mitophagy, we propose that pyruvate accumulation by PDK4 is essential for mitophagy. Especially, pyruvate is required for the stabilization of PINK1 on the OM of depolarized mitochondrion. Surprisingly, in the absence of pyruvate, the normal mitochondrial events occur even though cells were exposed to CCCP; PINK1 was imported into the IM of mitochondrion and degraded over there by proteasome.[42-44] In addition to a recent report that TOMM complexes are required for PINK1 stabilization by reciprocal interaction,[44] we suggests pyruvate as an enhancer for the interaction. Accordingly, pyruvate-mediated mitophagy belongs to canonical PINK1/PARK2 pathway by affecting PARK2 translocation onto depolarized mitochondria and subsequent recruitment of LC3. Unlike the protective effect of pyruvate on ischemic damage, pyruvate analogues did not rescue the mitophagy, indicating that the role of pyruvate in mitophagy was not attributable to anti-oxidation activity of pyruvate.

However, the effects of pyruvate on the mitophagy seemed to occur in a cell-type specific manner. Our results showed that PINK1 was stabilization by pyruvate in HeLa and HepG2, while it was not in HEK293T cells. In HEK293T cells, overexpression of PDK4 and pyruvate treatment still stimulated mitophagy, while pyruvate treatment did not affect PINK1 stabilization. Thus, pyruvate may not be the only factor regulating the stability of PINK1 and accompanying mitophagy and other mechanism may play a role in the PDK4-mediated mitophagy. A hypotheses might be possible for this phenomenon. Pyruvate-free DMEM, the culture medium we used, has high level of glucose that is actively metabolized via glycolysis pathway to produce pyruvate. While cells were incubated with pyruvate-free DMEM before the experiments, there might already be sufficient amount of pyruvate produced from the glycolysis pathway by the cell-type specific manner. Or, metabolic status or mitochondrial activity in addition to pyruvate may also contribute to the PDK4-mediated mitophagy. Identification of this pathway remains to be further addressed. Nonetheless, pyruvate was essential in the mitophagy in most of cells we examined.

Evaluation of pyruvate level should be considered to measure mitophagy in cell level or *in vivo*. Physiological concentration of pyruvate is approximately 0.1 to 0.2 mM[9] and the effective concentration of pyruvate in mitophagy we utilized in our assay was 1 mM. Given that pyruvate normally transverses blood brain barrier,[46] administration of pyruvate might be a candidate for mitochondrial defect-associated neurodegenerative disease, if proper half-life was determined. Our preliminary data indicate that pyruvate is involved in 1-methyl-4-phenylpyridinium (MPP+)-induced mitochondrial damage and cell death. Although the precise mechanism was remained to be elucidated, we propose PDK4 as major modulator of pyruvate that stabilizes PINK1 on the depolarized mitochondrion and thus activates mitophagy. Collectively from PARK1 and 2, I suggest an integrated model for mitophagy (**Fig. 9**).

# 5. REFERENCE

1. Ashrafi G, Schwarz TL. The pathways of mitophagy for quality control and clearance of mitochondria. Cell Death Differ 2013; 20:31-42.

2. Kanki T, Wang K, Cao Y, Baba M, Klionsky DJ. Atg32 is a mitochondrial protein that confers selectivity during mitophagy. Dev Cell 2009; 17:98-109.

3. Orvedahl A, Sumpter R, Jr., Xiao G, Ng A, Zou Z, Tang Y, et al. Image-based genome-wide siRNA screen identifies selective autophagy factors. Nature 2011; 480:113-7.

4. Hasson SA, Kane LA, Yamano K, Huang CH, Sliter DA, Buehler E, et al. High-content genome-wide RNAi screens identify regulators of parkin upstream of mitophagy. Nature 2013; 504:291-5.

5. Scarffe LA, Stevens DA, Dawson VL, Dawson TM. Parkin and PINK1: much more than mitophagy. Trends Neurosci 2014; 37:315-24.

6. Jin SM, Youle RJ. PINK1- and Parkin-mediated mitophagy at a glance. Journal of cell science 2012; 125:795-9.

7. Chu CT, Ji J, Dagda RK, Jiang JF, Tyurina YY, Kapralov AA, et al. Cardiolipin externalization to the outer mitochondrial membrane acts as an elimination signal for mitophagy in neuronal cells. Nature cell biology 2013; 15:1197-205.

8. Allen GF, Toth R, James J, Ganley IG. Loss of iron triggers PINK1/Parkin-independent mitophagy. EMBO Rep 2013; 14:1127-35.

9. Mallet RT, Sun J, Knott EM, Sharma AB, Olivencia-Yurvati AH. Metabolic cardioprotection by pyruvate: recent progress. Exp Biol Med (Maywood) 2005; 230:435-43.

10. Diers AR, Broniowska KA, Chang CF, Hogg N. Pyruvate fuels mitochondrial respiration and proliferation of breast cancer cells: effect of monocarboxylate transporter inhibition. Biochem J 2012; 444:561-71.

11. Herzig S, Raemy E, Montessuit S, Veuthey JL, Zamboni N, Westermann B, et al. Identification and functional expression of the mitochondrial pyruvate carrier. Science 2012; 337:93-6.

12. Bricker DK, Taylor EB, Schell JC, Orsak T, Boutron A, Chen YC, et al. A mitochondrial pyruvate carrier required for pyruvate uptake in yeast, Drosophila, and humans. Science 2012; 337:96-100.

13. Kaplon J, Zheng L, Meissl K, Chaneton B, Selivanov VA, Mackay G, et al. A key role for mitochondrial gatekeeper pyruvate dehydrogenase in oncogene-induced senescence. Nature 2013; 498:109-12.

14. Stacpoole PW. The pyruvate dehydrogenase complex as a therapeutic target for age-related diseases. Aging Cell 2012; 11:371-7.

15. Bindoli A, Barzon E, Rigobello MP. Inhibitory effect of pyruvate on release of glutathione and swelling of rat heart mitochondria. Cardiovasc Res 1995; 30:821-4.

16. Kerr PM, Suleiman MS, Halestrap AP. Reversal of permeability transition during recovery of hearts from ischemia and its enhancement by pyruvate. Am J Physiol 1999; 276:H496-502.

17. Rigobello MP, Bindoli A. Effect of pyruvate on rat heart thiol status during ischemia and hypoxia followed by reperfusion. Mol Cell Biochem 1993; 122:93-100.

18. DeBoer LW, Bekx PA, Han L, Steinke L. Pyruvate enhances recovery of rat hearts after ischemia and reperfusion by preventing free radical generation. Am J Physiol 1993; 265:H1571-6.

19. O'Donnell-Tormey J, Nathan CF, Lanks K, DeBoer CJ, de la Harpe J. Secretion of pyruvate. An antioxidant defense of mammalian cells. J Exp Med 1987; 165:500-14.

20. Constantopoulos G, Barranger JA. Nonenzymatic decarboxylation of pyruvate. Anal Biochem 1984; 139:353-8.

21. Roudier E, Perrin A. Considering the role of pyruvate in tumor cells during

hypoxia. Biochim Biophys Acta 2009; 1796:55-62.

22. Regitz V, Azumi T, Stephan H, Naujocks S, Schaper W. Biochemical mechanism of infarct size reduction by pyruvate. Cardiovasc Res 1981; 15:652-8.

23. Kristo G, Yoshimura Y, Niu J, Keith BJ, Mentzer RM, Jr., Bunger R, et al. The intermediary metabolite pyruvate attenuates stunning and reduces infarct size in in vivo porcine myocardium. Am J Physiol Heart Circ Physiol 2004; 286:H517-24.

24. Jeong JY, Jeoung NH, Park KG, Lee IK. Transcriptional regulation of pyruvate dehydrogenase kinase. Diabetes Metab J 2012; 36:328-35.

25. Roche TE, Baker JC, Yan X, Hiromasa Y, Gong X, Peng T, et al. Distinct regulatory properties of pyruvate dehydrogenase kinase and phosphatase isoforms. Prog Nucleic Acid Res Mol Biol 2001; 70:33-75.

26. Patel MS, Korotchkina LG. Regulation of the pyruvate dehydrogenase complex. Biochem Soc Trans 2006; 34:217-22.

27. Gudi R, Bowker-Kinley MM, Kedishvili NY, Zhao Y, Popov KM. Diversity of the pyruvate dehydrogenase kinase gene family in humans. J Biol Chem 1995; 270:28989-94.

28. Rowles J, Scherer SW, Xi T, Majer M, Nickle DC, Rommens JM, et al. Cloning and characterization of PDK4 on 7q21.3 encoding a fourth pyruvate dehydrogenase kinase isoenzyme in human. J Biol Chem 1996; 271:22376-82.

29. Wu P, Sato J, Zhao Y, Jaskiewicz J, Popov KM, Harris RA. Starvation and diabetes increase the amount of pyruvate dehydrogenase kinase isoenzyme 4 in rat heart. Biochem J 1998; 329 ( Pt 1):197-201.

30. Wu P, Inskeep K, Bowker-Kinley MM, Popov KM, Harris RA. Mechanism responsible for inactivation of skeletal muscle pyruvate dehydrogenase complex in starvation and diabetes. Diabetes 1999; 48:1593-9.

31. Holness MJ, Smith ND, Bulmer K, Hopkins T, Gibbons GF, Sugden MC. Evaluation of the role of peroxisome-proliferator-activated receptor alpha in the regulation of cardiac pyruvate dehydrogenase kinase 4 protein expression in response to starvation, high-fat feeding and hyperthyroidism. Biochem J 2002; 364:687-94.

32. Jeoung NH, Wu P, Joshi MA, Jaskiewicz J, Bock CB, Depaoli-Roach AA, et al. Role of pyruvate dehydrogenase kinase isoenzyme 4 (PDHK4) in glucose homoeostasis during starvation. Biochem J 2006; 397:417-25.

33. Jeoung NH, Harris RA. Pyruvate dehydrogenase kinase-4 deficiency lowers

blood glucose and improves glucose tolerance in diet-induced obese mice. Am J Physiol Endocrinol Metab 2008; 295:E46-54.

34. Lee FN, Zhang L, Zheng D, Choi WS, Youn JH. Insulin suppresses PDK-4 expression in skeletal muscle independently of plasma FFA. Am J Physiol Endocrinol Metab 2004; 287:E69-74.

35. Guo L, Xie B, Mao Z. Autophagy in Premature Senescent Cells Is Activated via AMPK Pathway. Int J Mol Sci 2012; 13:3563-82.

36. Pyo JO, Nah J, Kim HJ, Lee HJ, Heo J, Lee H, et al. Compensatory activation of ERK1/2 in Atg5-deficient mouse embryo fibroblasts suppresses oxidative stress-induced cell death. Autophagy 2008; 4:315-21.

37. Park S, Choi SG, Yoo SM, Son JH, Jung YK. Choline dehydrogenase

interacts with SQSTM1/p62 to recruit LC3 and stimulate mitophagy. Autophagy 2014; 10.

38. Zhao G, Jeoung NH, Burgess SC, Rosaaen-Stowe KA, Inagaki T, Latif S, et al. Overexpression of pyruvate dehydrogenase kinase 4 in heart perturbs metabolism and exacerbates calcineurin-induced cardiomyopathy. Am J Physiol Heart Circ Physiol 2008; 294:H936-43.

39. Melser S, Chatelain EH, Lavie J, Mahfouf W, Jose C, Obre E, et al. Rheb regulates mitophagy induced by mitochondrial energetic status. Cell Metab 2013; 17:719-30.

40. Novak I, Kirkin V, McEwan DG, Zhang J, Wild P, Rozenknop A, et al. Nix is a selective autophagy receptor for mitochondrial clearance. EMBO Rep 2010; 11:45-51.

41. Ding WX, Ni HM, Li M, Liao Y, Chen X, Stolz DB, et al. Nix is critical to two distinct phases of mitophagy, reactive oxygen species-mediated autophagy induction and Parkin-ubiquitin-p62-mediated mitochondrial priming. J Biol Chem 2010; 285:27879-90.

42. Fedorowicz MA, de Vries-Schneider RL, Rub C, Becker D, Huang Y, Zhou C, et al. Cytosolic cleaved PINK1 represses Parkin translocation to mitochondria and mitophagy. EMBO Rep 2014; 15:86-93.

43. Jin SM, Lazarou M, Wang C, Kane LA, Narendra DP, Youle RJ. Mitochondrial membrane potential regulates PINK1 import and proteolytic destabilization by PARL. J Cell Biol 2010; 191:933-42.

44. Lazarou M, Jin SM, Kane LA, Youle RJ. Role of PINK1 binding to the

TOM complex and alternate intracellular membranes in recruitment and activation of the E3 ligase Parkin. Dev Cell 2012; 22:320-33.

45. Morishige Y, Fujimori K, Amano F. Differential resuscitative effect of pyruvate and its analogues on VBNC (viable but non-culturable) Salmonella. Microbes Environ 2013; 28:180-6.

46. Choi BY, Kim JH, Kim HJ, Yoo JH, Song HK, Sohn M, et al. Pyruvate administration reduces recurrent/moderate hypoglycemia-induced cortical neuron death in diabetic rats. PloS one 2013; 8:e81523.

# 국문 초록

## 피루브산이 Mitophagy 과정에서 PINK1 안정화에 미치는 영향

손상된 미토콘드리아는 autophagy 기작에 의해 제거되는데, 이를 mitophagy라 한다. Mitophagy의 분자적 조절 기작을 밝히려는 많은 노력에도 불구하고, 아직도 많은 부분이 미해결 과제로 남아있다. 본 연구에서는, 세포를 기반으로 한 형광 검출 방법과 미토콘드리아 cDNA library를 사용하여 CCCP에 의해 유도되는 mitophagy를 조절하는 유전자를 스크리닝 하였고, PDK4를 동정하였다. PDK4는 세포질과 미토콘드리아에서 피루브산의 양을 증가시켰고, 이는 탈분극된 미토콘드리아에서 PINK1 단백질의 안정화에 필요함을 관찰하였다. 피루브산이 결핍된 조건에서는 미토콘드리아의 제거가 잘 일어나지 않았다. 피루브산을 매개해서 일어나는 mitophagy는 산화적 인산화나 세포내 ATP 양과는 무관하였고, 따라서 세포내 에너지 대사와는 무관함을 의미한다. 대신에 CCCP 조건에서 PINK1이 TOMM 중합체와

결합하는데 중요한 역할을 함으로써 PINK1의 안정화에 영향을 주고 있음을 밝혔다. 또한, 피루브산은 mitophagy의 다음 기작인 PARK2와 LC3가 미토콘드리아로 이동하는데도 영향을 주고 있었다. 따라서, 본 연구는 피루브산이 CCCP에 의해 유도되는, PINK1/PARK2에 의한 mitophagy에 중요한 역할을 함을 규명하였다.